Solid Earth Discuss., 5, 1941–2004, 2013
www.solid-earth-discuss.net/5/1941/2013/
doi:10.5194/sed-5-1941-2013

Solid Earth
Discussions
Open Access

Jurassic–Paleogene intra-oceanic magmatic evolution of the Ankara Mélange, North-Central Anatolia, Turkey

E. Sarifakioglu[1], Y. Dilek[2], and M. Sevin[1]

[1]General Directorate of Mineral Reseach & Exploration, Department of Geology, 06520 Ankara, Turkey
[2]Department of Geology & Env. Earth Science, Miami University, Oxford, OH 45056, USA

Received: 11 September 2013 – Accepted: 16 September 2013
– Published: 13 November 2013

Correspondence to: E. Sarifakioglu (esarifakioglu@mta.gov.tr) and Y. Dilek (dileky@miamioh.edu)

Published by Copernicus Publications on behalf of the European Geosciences Union.

Abstract

Oceanic rocks in the Ankara Mélange along the Izmir–Ankara–Erzincan suture zone (IAESZ) in North-Central Anatolia include locally coherent ophiolite complexes (~179 Ma and ~80 Ma), seamount or oceanic plateau volcanic units with pelagic and reefal limestones (96.6 ± 1.8 Ma), metamorphic rocks with ages of 187.4 ± 3.7 Ma, 158.4 ± 4.2 Ma, and 83.5 ± 1.2 Ma, and subalkaline to alkaline volcanic and plutonic rocks of an island arc origin (~67–63 Ma). All but the arc rocks occur in a shaly-graywacke and/or serpentinite matrix, and are deformed by south-vergent thrust faults and folds that developed in the Middle to Late Eocene due to continental collisions in the region. Ophiolitic volcanic rocks have mid-ocean ridge (MORB) and island arc tholeiite (IAT) affinities showing moderate to significant LILE enrichment and depletion in Nb, Hf, Ti, Y and Yb, which indicate the influence of subduction-derived fluids in their melt evolution. Seamount/oceanic plateau basalts show ocean island basalt (OIB) affinities. The arc-related volcanic rocks, lamprophyric dikes and syeno-dioritic plutons exhibit high-K shoshonitic to medium-to high-K calc-alkaline compositions with strong enrichment in LILE, REE and Pb, and initial ε_{Nd} values between +1.3 and +1.7. Subalkaline arc volcanic units occur in the northern part of the mélange, whereas the younger alkaline volcanic rocks and intrusions (lamprophyre dikes and syeno-dioritic plutons) in the southern part. The Early to Late Jurassic and Late Cretaceous epidote-actinolite, epidote-chlorite and epidote-glaucophane schists represent the metamorphic units formed in a subduction channel in the Northern Neotethys. The Middle to Upper Triassic neritic limestones spatially associated with the seamount volcanic rocks indicate that the Northern Neotethys was an open ocean with its MORB-type oceanic lithosphere by the Early Triassic. The Latest Cretaceous–Early Paleocene island arc volcanic, dike and plutonic rocks with subalkaline to alkaline geochemical affinities represent intraoceanic magmatism that developed on and across the subduction-accretion complex above a N-dipping, southward-rolling subducted lithospheric slab within the

SED
5, 1941–2004, 2013

Northern Neotethys. The Ankara Mélange thus exhibits the record of ~120–130 million years of oceanic magmatism in geological history of the Northern Neotethys.

1 Introduction

In this paper we document the internal structure of the Ankara Mélange along the IAESZ in North-Central Anatolia, and present new geochemical and geochronological data from various magmatic rock assemblages that make up distinct tectonic units in this mélange. Our geochemical data and interpretations indicate that all units within the Ankara Mélange are intraoceanic in origin and appear to have formed during the seafloor spreading, seamount volcanism and island arc magmatism stages of the Northern Neotethys. We also present new Pb–Sr–Nd isotopic compositional data, and radiometric data belonging to both magmatic arc rocks and basic rocks from the Ankara Mélange. Thus, the Ankara Mélange displays a complete record of ~120–130 m.y. of intraoceanic magmatism that took place prior to the continental collisional events in Anatolia in the Eocene.

2 Regional geology

The IAESZ forms the tectonic boundary between the Pontide tectonic belt (including the Sakarya Continent) in the north and the Anatolide–Tauride block (including the CACC) in the south. The suture zone is marked by ophiolite units, ophiolitic mélanges, and seamount fragments. The Sakarya Continent in the Pontides represents the southern margin of Eurasia (Figs. 1 and 2). Carboniferous (330–310 Ma), high-grade metamorphic rocks (gneiss, migmatite, amphibolite and marble), currently exposed in the Kazdağ, Söğüt, Devrekani, and Pulur massifs (from west to east), make up the continental basement of the Sakarya Continent (Topuz et al., 2004, 2006; Okay et al., 2006; Nzegge et al., 2006). These metamorphic basement rocks are intruded by the Carboniferous (295 Ma) granitoids (Çoğulu et al., 1965; Delaloye and Bingöl, 2000). The

SED
5, 1941–2004, 2013

Triassic Karakaya Complex, representing a subduction-accretion complex, tectonically overlies the crystalline basement units (Tekeli, 1981). It includes the Lower Karakaya, which comprises metabasite, marble and phyllite rocks, and the Upper Karakaya consisting mainly of unmetamorphosed clastic and basic volcanic rocks with blocks of Carboniferous and Permian neritic limestones (Bingöl et al., 1975; Okay et al., 2002; Okay and Göncüoğlu, 2004).

The CACC consists mainly of Paleozoic–Mesozoic metamorphic massifs (Kırşehir, Akdağ, and Niğde massifs) and Cretaceous–Paleocene granitoids (Fig. 2). The metamorphic massifs comprise metacarbonate, metapelite and amphibolite-gneiss rocks that are the products of varied P/T conditions of metamorphism (Whitney and Dilek, 1998). The Late Cretaceous granitoids and the Eocene–Upper Miocene volcanic rocks crosscut and overlie (respectively) the crystalline basement units of the CACC (Güleç, 1994; Boztuğ, 2000; Kadıoğlu et al., 2003, 2006; İlbeyli et al., 2004). The Late Cretaceous plutons are composed of *Granite*, *Monzonite* and *Syenite Supersuites* with ages of 77.7 ± 0.3 Ma, 70 ± 1.0 Ma and 69.8 ± 0.3 Ma, respectively (Kadıoğlu et al., 2006). They display a chemical progression from high-K calc-alkaline and high-K shoshonitic to alkaline compositions, representing the development of within-plate magmatism across the CACC with time (Kadıoğlu et al., 2006).

3 Internal structure and tectonic units of the Ankara Mélange

The most important component of the IAESZ in its central segment in northern Anatolia is the Ankara Mélange, extending from Ankara in the west to Çorum in the east (Fig. 2). The Ankara Mélange is a well known subduction-accretion complex (Bailey and McCallien, 1950, 1953), consisting of blocks of Paleozoic limestone and metamorphic rocks, Jurassic–Cretaceous ophiolitic units, and Jurassic–Cretaceous seamount volcanic assemblages in a shaly-graywacke and/or serpentinite matrix (Figs. 3 and 4; Norman, 1984; Akyürek et al., 1984; Koçyiğit, 1991; Tüysüz et al., 1995; Tankut et al., 1998; Dilek and Thy, 2006; Dangerfield et al., 2011).

SED
5, 1941–2004, 2013

Megablocks and imbricated thrust sheets of oceanic rocks occur as mappable units enveloped in a pelitic (clayey, sandy-silty), serpentinite or volcanic matrix within the Ankara Mélange (Fig. 5). In some of these blocks or thrust sheets the mafic-ultramafic rock units and the associated sedimentary rocks make up coherent ophiolite complexes (e.g. the Eldivan ophiolite) (Figs. 6 and 7), representing the Neotethyan oceanic lithosphere. Plagiogranite dikes intruding the serpentinized peridotites near Eldivan (Çankırı) revealed U–Pb zircon ages of 179 Ma (Dilek and Thy, 2006), indicating that part of the Neotethyan oceanic crust preserved in the mélange is as old as the Early Jurassic. The radiolarian fauna in the chert blocks have yielded Late Carnian–Middle Norian, and Middle Jurassic to Middle Cretaceous ages (Sarifakioglu et al., unpublished data). However, the whole-rock $^{40}Ar/^{39}Ar$ dating of basaltic pillow lava from an ophiolitic thrust sheet farther south in the Ankara Mélange has revealed an age of 80.3 ± 7.6 Ma, indicating that Late Cretaceous oceanic crustal rocks also exist within the mélange (Table 1).

The Senomanian–Santonian flyschoidal sedimentary rocks with pebblestone, sandstone, mudstone and clayey limestone with interbedded chert layers unconformably rest on the ophiolitic rocks (Figs. 3 and 4). However, Kimmeridgian–Hauterivian flyschoidal sedimentary rocks cover the ophiolitic pillow lavas father south in the Ankara Mélange (Sarifakioglu et al., unpublished data). The Upper Santonian–Maastrichtian, thin- to medium-layered clayey to sandy limestone and volcanic detrital rocks rest unconformably on these flyschoidal sedimentary and ophiolitic rocks around Yapraklı (Çankırı) and Laloğlu (Çorum), and represent the forearc basin strata (Figs. 6 and 7). The ophiolitic, flyschoidal and forearc basin rocks are imbricated along south-directed thrust faults (Sarifakioglu et al., 2011).

Blocks (km-size) of alkaline volcanic and pyroclastic rocks, debris flow deposits, and coarse-grained reefal limestones representing seamount and/or oceanic plateau fragments also occur in the Ankara Mélange (Fig. 8). We have obtained Middle–Upper Triassic and Cretaceous biostratigraphic ages from the reefal limestones overlying the seamount volcanic units, and $^{40}Ar/^{39}Ar$ whole-rock ages of 96.6 ± 1.8 Ma from the al-

SED
5, 1941–2004, 2013

kaline pillow lavas that are stratigraphically associated with the pink colored pelagic limestones (Sarifakioglu et al., unpublished data). Rojay et al. (2004) obtained the Late Barremian–Early Aptian biostratigraphic ages from the reefal limestones resting on the pillow lavas with ocean island basalt (OIB) geochemical affinities. Blocks of these neritic carbonates and the underlying alkaline pillow lavas are also embedded in a turbiditic sequence consisting of chert and volcanic rock clasts in a fine-grained sandstone matrix. Volcanic debris flow deposits also occur within the turbiditic sequence.

In addition to the blocks of ophiolitic, seamount and oceanic plateau rocks, the Ankara Mélange also contains blocks of metamorphic rocks, mainly epidote-glaucophane, epidote-chlorite, and epidote-actinolite schists (Fig. 6). The geochemical fingerprinting of these rocks suggests that their protoliths were made of seamount volcanics and ophiolitic basic rocks, and related sediments. Detailed descriptions and documentation of these metamorphic rocks will be presented elsewhere. We interpret these metamorphic rocks to have formed in an intra-oceanic subduction zone. The ^{40}Ar–^{39}Ar dating of the epidote-glaucophane, epidote-chlorite and epidote-actinolite schists revealed the cooling ages of 83.5 ± 1.2 Ma, 158.4 ± 4.2 Ma, and 187.4 ± 3.7 Ma, respectively whereas phyllite, actinolite schist and amphibole-epidote schist yielded 119.8 ± 3.3 Ma, 177.4 ± 5.8 Ma, 256.9 ± 8.0 Ma, respectively (Tables 2 and 3).

Overlying the Ankara Mélange tectonically or unconformably are volcanic and volcaniclastic rocks of an island arc origin (Figs. 9 and 10). Nearly 20 km north of Kalecik subalkaline to alkaline volcanic rocks (Dönmez et al., 2009), intercalated with clayey and sandy limestone, calcareous sandstone, pebblestone, sandstone and shale, overlie the Ankara Mélange units and the flyschoidal sedimentary rocks (Hakyemez et al., 1986; Rojay and Süzen, 1997). The volcanic rocks are locally overlain by the Upper Cretaceous reefal limestones and sandstones containing rudist fossils (Fig. 10a and b). Both pillowed and massive lava flows with cooling joints occur (Figs. 9c and 10d); the massive lava flows contain cm-size augite and leucite phenocrysts. Mafic dikes locally crosscut the volcaniclastic rocks of the arc sequence (Fig. 9d). The ^{40}Ar–^{39}Ar whole-rock dating of an arc-related pillow lava has yielded an age of 67.8 ± 4.9 Ma (Table 4a).

SED
5, 1941–2004, 2013

Lamprophyre dikes and a syeno-diorite pluton of an island arc origin are intruded into the ophiolitic and seamount rocks and the mélange matrix along the Kizilirmak River near and east of Kalecik (Fig. 11). The brownish grey colored lamprophyric dikes continue along-strike for 200 to 1000 m, and are displaced by local thrust faults. The ^{40}Ar–^{39}Ar whole-rock dating and the ^{40}Ar–^{39}Ar biotite age from the lamprophyric dikes revealed ages of 67.2 ± 1.2 Ma an 63.6 ± 1.2 Ma, respectively (Table 4b and c).

We have also obtained an ^{40}Ar–^{39}Ar biotite age of 75.9 ± 1.3 Ma from a syeno-dioritic pluton, approximately 1 km in diameter, indicating that the arc magmatism started as early as the Campanian and that it progressed with alkaline volcanism and dike emplacement throughout the Maastrichtian and Early Paleocene (Table 4d). Andesitic lavas and volcaniclastic and pyroclastic rocks are intercalated with the Upper Cretaceous–lower Paleocene turbiditic rocks in the region. These turbiditic and flyschoidal rocks contain volcanic pebbles in the lower stratigraphic levels and grade upwards into sandstone and shale. The Paleocene rocks (Dizilitaslar Formation) are conformably overlain by the lower to Middle Eocene sandstone, shale, clayey limestone and marl units that collectively make up the Mahmutlar Formation (Akyürek et al., 1984). All these Paleogene sedimentary rocks were deformed by south-vergent thrust faults and folds, indicating that they underwent N–S-directed contractional deformation in the Middle to Late Eocene.

4 Petrography

In this section we describe the primary and secondary mineral assemblages and the textures of the main lithological types associated with the Neotethyan oceanic crust, seamount volcanic units, and island arc assemblages (e.g. volcanic rocks, lamprophyre dikes and syeno-diorite plutons) that we investigated in the study area.

SED
5, 1941–2004, 2013

4.1 Basalt

The seamount-related alkaline basaltic rocks consist mainly of plagioclase (55–60 %) and clinopyroxene (approximately 40 %), displaying an intergranular texture (Fig. 12a). Some of the basalt samples contain olivine phenocrysts (about 15 %) ranging in size from 0.2 mm to 2 mm. Clinopyroxene grains (titanaugites) are partially altered into chlorite, olivine to serpentine and iddingsite, and plagioclase to sericite and chlorite. Apatite and opaque minerals (Fe–Ti oxide) occur as accessory minerals. Amygdals are filled with secondary carbonate and chlorite minerals.

Tholeiitic basaltic rocks of the Neotethyan oceanic crust comprise microlitic plagioclase and clinopyroxene crystals in a fine-grained texture (Fig. 12b). They are partially or completely spilitized, with plagioclase replaced by albite, sericite, chlorite and epidote (saussuritization), whereas clinopyroxene replaced by actinolite (uralitization) and chlorite. The glassy material in the matrix is transformed into chlorite. Leucoxene and opaque minerals are present as accessories. Vesicles in the basaltic lavas are filled by secondary carbonate and chlorite.

The island-arc basaltic rocks consist mainly of plagioclase (about 55 %) and clinopyroxene (45 %) crystals in the porphyritic textures with chloritized glassy and microcrystalline groundmass. Clinopyroxene (diopside) grains range in size from 0.2 mm to 2 mm in length (Fig. 12c and d), and locally display twinning. The plagioclases are partly altered to chlorite and carbonate minerals. Accessory minerals are made of fine crystalline Fe–Ti oxides. Basaltic andesites contain plagioclase, clinopyroxene, minor olivine and biotite within porphyritic and glomeroporphyritic textures (Fig. 12e). Ferromagnesium minerals are locally 1.5 cm-long. Fe–Ti oxide minerals are accessories. The groundmass consists of plagioclase microlites, and chloritized and/or devitrified glass. Basaltic lavas include vesicles filled by secondary carbonate, chlorite, and zeolite.

SED
5, 1941–2004, 2013

4.2 Basanite

The ultrabasic volcanic rocks consist of clinopyroxene, plagioclase and minor olivine occurring as euhedral and subhedral grains in a hyalomicrolitic, porphyritic texture. Plagioclase forms microlites or micro-phenocrysts, and is commonly altered to clay minerals. Clinopyroxene is mainly augite, and displays zoning and twinning. Olivine is surrounded by a groundmass that is made entirely of serpentine minerals. Small analcime crystals occur as a replacement of leucite between plagioclase and clinopyroxene crystals within the groundmass.

4.3 Tephrite

This fine-grained basaltic rock comprises clinopyroxene (augite), leucite, rare olivine and black mica (phlogopite) crystals within a hyalomicrolitic or porphyritic texture. Plagioclase microlites, ultra fine-grained clinopyroxene, phlogopite, leucite and glassy material form the groundmass, whereas clinopyroxene and leucite occur as euhedral to subhedral microphenocrysts. The leucite contents in the leucite-tephrite rock are up to ~25 % (Fig. 12d). Small, anhedral or subhedral opaque minerals are found as accessory minerals.

Some tephrites display characteristic features of phonolitic tephrite with feldspar crystals (plagioclase > K-feldspar) and mafic minerals (phlogopite, hornblende) in a microcrystalline porphyritic texture. Plagioclase is partially altered to sericite and chlorite, whereas sanidine is partially altered to sericite and clay minerals. Leucite occurs as subhedral grains, is mostly altered to sanidine microlites, zeolite and clay minerals, and is surrounded by small phlogopite flakes. Euhedral apatite crystals and anhedral opaque minerals (Fe–Ti oxides) are present as accessories.

SED
5, 1941–2004, 2013

4.4 Lamprophyre

These alkaline dike rocks consist mainly of small prismastic clinopyroxene (diopside), minor phlogopite and leucite pseudomorphs embedded in a groundmass composed of feldspars (orthoclase > plagioclase), analcime crystals and glassy material (Fig. 12f and g). Both plagioclase and orthoclase are partly or completely altered to carbonate, clay and zeolite minerals; phlogopite is replaced by chlorite along its rims. Small, interstitial apatite laths are enclosed in the orthoclase crystals. In addition, euhedral prismatic apatite crystals up to 0.7 mm in length are also present in the groundmass. Opaque minerals occur as accessory crystals.

4.5 Syeno-diorite

The main minerals in this intrusive rock include feldspar (plagioclase ≥ orthoclase), clinopyroxene, hornblende and biotite (Fig. 12h). Subhedral to anhedral plagioclase crystals form a granular texture; some large orthoclase crystals (~2.5 cm) locally give the rock a porphyry texture. Plagioclase grains (An_{28}–An_{48}) are locally surrounded by orthoclase. K-feldspar grains display a perthitic texture. Subhedral to anhedral clinopyroxene (diopside), hornblende and biotite crystals show partial chloritization. Subhedral hornblende crystals have opacite rims around them as a result of metasomatism during their reaction with melt (Plechov et al., 2008). The subhedral prismatic apatite and anhedral granular opaque minerals are present as accessories.

5 Analytical methods

We analyzed fifthy-one (51) rock samples for major, trace, and rare-earth element chemistry at ACME Analytic Laboratory (Canada). Inductively coupled plasma-emission spectroscopy has been used for major-element analysis, and inductively coupled plasma-mass spectroscopy has been used for the analysis of both trace elements

SED
5, 1941–2004, 2013

and rare-earth elements (REE). The results of these analyses are presented in Tables 5, 6, 7, 8 and 9.

$^{40}Ar/^{39}Ar$ age dating was done at the Geochronology and Isotopic Geochemistry Laboratory of Activation Laboratories Ltd. (Actlabs), Ancaster, Ontario, Canada. We obtained $^{40}Ar/^{39}Ar$ ages of biotite separates from two samples of the arc rocks. In addition, whole rock fractions of five rock samples were analyzed. The samples wrapped in Al foil was loaded in evacuated and sealed quartz vial with K and Ca salts and packets of LP–6 biotite interspersed with the samples to be used as a flux monitor. The sample was irradiated in the nuclear reactor for 48 h. The flux monitors were placed between every two samples, thereby allowing precise determination of the flux gradients within the tube. After the flux monitors were run, J values were then calculated for each sample, using the measured flux gradient. LP–6 biotite has an assumed age of 128.1 Ma. The neutron gradient deed not exceeded 0.5 % on sample size. The Ar isotope composition was measured in a Micromass 5400 static mass spectrometer. 1200 °C blank of ^{40}Ar deed not exceed $n \times 10^{-10}$ cc STP.

Argon is extracted from the sample as degassing at ~100 °C during two days in double vacuum furnace at 1700 °C. Argon concentration is determined using isotope dilution with ^{38}Ar spike, which is introduced to the sample system prior to each extraction. The obtained pure Ar is introduced into customer build magnetic sector mass spectrometer (Reinolds type) with Varian CH5 magnet. Measurement Ar isotope ratios is corrected for mass-discrimination and atmospheric argon assuming that ^{36}Ar is only from the air. After each analysis the extraction temperature is elevated to 1800 °C for few minutes. Then, Aliquot of the sample is weighted into graphite crucible with lithium metaborate/tetraborate flux and fussed using LECO induction furnace for K-analysis. The fusion bead is dissolved with acid. Standards, blanks and sample are analyzed on Thermo Jarrell Ash Enviro II ICP Spectrometer.

The Sr, Nd, and Pb isotopic compositions of six samples from the alkaline lamprophyric dikes have been determined at the ACT Analytical Laboratories Ltd., Canada (Table 9). The Sr isotope analysis was performed with a Triton multi-collector mass-

SED
5, 1941–2004, 2013

spectrometer in static mode. The weighted average of 15 SRM–987 Sr-standard runs yielded 0.710258 ± 9 (2 s) for $^{87}Sr/^{86}Sr$. Sm and Nd were separated by extraction chromatography on hexyl di-ethyl hydrogen phosphate-covered Teflon powder. The analysis was performed on a Triton multi-collector mass spectrometer in static mode. $^{143}Nd/^{144}Nd$ ratios are relative to the value of 0.511860 for the La Jolla standard. Pb was separated using the ion-exchange technique with Bio–Rad 1 × 8. Pb isotope compositions were analyzed on Finnigan MAT–261 multicollector mass spectrometer. The measured Pb isotope ratios were corrected for mass fractionation calculated from replicate measurements of Pb isotope composition in the National Bureau of Standards SRM – 982 standards. External reproducibility of lead isotope ratios – $^{206}Pb/^{204}Pb = 0.1\,\%$, $^{207}Pb/^{204}Pb = 0.1\,\%$, $^{208}Pb/^{204}Pb = 0.2\,\%$ – on the 2σ level has been demonstrated through multiple analyses of standard BCR–1.

6 Geochemistry

We report below on the geochemistry of the representative samples of oceanic basaltic rocks in the Ankara Mélange, as well as the lamprophyric dikes, a syeno-dioritic pluton, and alkaline lavas that crosscut and/or cover the blocks of volcanic and volcaniclastic rocks, serpentinite, radiolarian chert, and shale in the Ankara Mélange.

6.1 Oceanic basaltic rocks

The $Na_2O_2 + K_2O$ values of basaltic blocks of the Neotethyan oceanic crust range from 1 wt % to 4.28 wt %, with the K_2O values much lower than those of Na_2O (Table 5). The Na enhancement of two samples (CE.07, CE.08) may be a result of spilitization caused by low-grade hydrothermal ocean floor metamorphism. Similarly, the total alkali values from the seamount volcanic blocks vary between 4.72 and 8.14 wt %, with the Na_2O values (3.78–6.79 wt %) much higher than that of oceanic crust (Table 6).

SED
5, 1941–2004, 2013

On the total alkali vs. silica (TAS) diagram the tholeiitic-calcalkaline volcanic and isolated dike rocks from the Tethyan oceanic crust fall in the field of basalt and basaltic andesite, whereas the samples of seamount alkaline rocks plot in the basanite, tephrite (SiO_2 = 39.77–46.36 wt %), trachyte (SiO_2 = 68.47 wt %), trachybasalt (SiO_2 = 50.15 wt %) and foidite (SiO_2 = 39.77 wt %) fields (Fig. 13a and b). The oceanic basalt samples have lower TiO_2 values (0.26–1.74 wt %) in comparison to the alkaline, seamount volcanic rocks (1.64–2.46 wt %), except for a volcanic sample with tholeiitic OIB (Ocean–Island basalt) characteristics. On a Ti–Zr–Y discrimination diagram (Pearce and Cann, 1973), the oceanic basalt samples plot in the MORB (mid-ocean ridge basalt) and island arc tholeiite (IAT) fields, whereas the seamount volcanic rocks generally fall in the within-plate alkali basalt field (except a trachyte sample; Fig. 13c). On a Ti–V diagram (Shervais, 1982), the samples of oceanic basaltic rocks mostly plot in the MORB field (Ti/V = 22.6–28.9), whereas four samples have island arc tholeiite to boninitic affinities (Ti/V = 5.4–25.55) (Fig. 13d). The samples of silica-undersaturated, seamount volcanic rocks display an OIB–character with high Ti/V ratios (62.6–261.2).

The N-MORB normalized multi-element diagrams of the representative samples of basalts of oceanic crust and seamount volcanic rocks are shown in Fig. 13e. Basaltic samples of both MORB and SSZ (suprasubduction zone) affinities show enrichment in their LILE (the large ion lithophile elements: Rb, Ba, K, Sr, Cs, Th) contents. The HFSE (high field strength elements: Nb, Ta, Zr, Hf, Ti, Y) and REE (rare earth elements) contents of the MORB-type basaltic rocks display a slight increase, whereas the SSZ-related basaltic rocks (four samples) exhibit depletion in HFSE and REE. The LILE, HFSE, LREE (light–REE) contents of the seamount volcanic rocks are extremely enriched relative to the HREE (heavy–REE) values. Also, the Th/Yb (2.8–5.6) and Nb/Yb (27.6–54.8) values of the seamount volcanic rocks are high in comparison to those of the Neotethyan oceanic basalt samples (Th/Yb = 0.2–1.1; Nb/Yb = 0.7–2.7). However, the alkaline lava samples have the ratios of Nb/Y > 1.5 and Zr/Nb < 6 that are typical for within-plate basalts (Edwards et al., 1991). The seamount volcanic rocks have

SED
5, 1941–2004, 2013

Nb/Y ratios of 2.3–3.1 and Zr/Nb ratios of 3.1–4.1, indicating OIB-like geochemical characteristics, whereas the oceanic basalt samples have Nb/Y (0.1–0.4) and Zr/Nb (8.1–32) values characteristic of island-arc rocks.

6.2 Island arc rocks

A small syeno-diorite pluton, a suite of volcanic rocks, and lamprophyric dikes in the Kalecik (Ankara) area collectively represent the products of island arc magmatism. These arc rocks mostly plot in the alkaline field on a TAS diagram (Fig. 14a and b).The alkaline rock samples with medium to high Al_2O_3 contents (10–19 wt %) represent both silica-saturated and silica-undersaturated rock units (Tables 7, 8 and 9). The lamprophyric dikes have picrobasalt, trachybasalt, trachyandesite, tephrite and phonotephrite compositions, whereas the volcanic rocks display basalt, basanite, tephrite, leucite tephrite and foidite compositions. The samples from small alkaline intrusions fall into the syeno-diorite field in the TAS diagram (Fig. 14b; Cox et al., 1979). The Late Cretaceous–Early Paleocene volcanic rocks (andesite, dacite, rhyolite), found nearly 60 km SW of Kalecik, show subalkaline (tholeiitic and calc-alkaline) compositions, except for a few trachytbasalt and trachyandesite samples (Fig. 14a, c and d; Dönmez et al., 2009).

The alkaline volcanic rocks mostly display high-K shoshonitic compositions in the K_2O vs. Si_2O diagram (Fig. 14d; Peccerillo and Taylor, 1976). Some volcanic and dike rocks also plot in the fields of medium–high-K, calc-alkaline series. Although some alkaline volcanic rocks show medium-K calc-alkaline characteristics as a result of hydrotermal alteration (LOI/loss on ignition > 2 wt %), they have high-K shoshonitic affinity since the leucite bearing, silica-undersaturated alkaline rocks experienced analcimization resulting in low K_2O values in favor of Na_2O values. On the Hastie et al. (2007), and Pearce (1982) diagrams, which utilize the immobile elements and the ratios of immobile elements (Th vs. Co, and Ce/Yb vs. Ta/Yb), the arc-related plutonic, volcanic and dike rocks generally display high-K (K_2O/Na_2O = 1.5–3.4) and shoshonitic characteristics (Fig. 14e and f). However, seven samples from the volcanic rocks and

SED
5, 1941–2004, 2013

lamprophyre dikes contain high K_2O/Na_2O ratios (18.16–24.52) showing ultrapotassic ($K_2O/Na_2O > 3$) characteristics.

When plotted on MgO vs. major element diagrams, the analyzed samples mainly exhibit negative correlations, except on the Fe_2O_3 and TiO_2 plots, which show positive correlations (Fig. 15). Based on the MgO vs. trace element variation diagrams (Fig. 15), Co shows a positive trend while Ba, Rb, Sr, Th and Zr all exhibit negative trends. These major and trace element trends can be explained by fractionation crystallization of clinopyroxene, feldspar, black mica (biotite, phlogopite), Fe–Ti oxides and apatite. However, the scatter in Fig. 15 may also be caused by the alteration of the arc rocks and/or the involvement of subducted sediments in their melt regime. The rock samples from the small syeno-diorite pluton with metaluminous characteristics plot in the VAG (volcanic arc granites) field (Fig. 16a, b and c). The Ti–Zr–Y and Ti–V diagrams (Pearce and Cann, 1973; Shervais, 1982) show that the alkaline basic samples and the subalkaline volcanic rocks (Dönmez et al., 2009) from the southwestern part of the study area all plot in the arc field (Fig. 16d and e), whereas the TiO_2–Al_2O_3 and Y–Zr diagrams (Muller et. 1992) show that these samples fall into the arc field (Fig. 16f and g). The analyzed alkaline rocks display shoshonitic characteristics in the Th/Yb vs. Nb/Yb diagram (Pearce, 2008), and their Hf/Th ratios are rather low ranging from 0.11 to 0.57, consistent with their shoshonitic affinity. The island-arc tholeiitic (IAT) basaltic rocks have $Hf/Th > 3$, whereas the calc-alkaline volcanic rocks have $Hf/Th < 3$ (Wood, 1980). Their Th enrichment and increased Th/Yb ratios along the mantle metasomatism trend indicate the influence of subduction-derived fluids in their magma source (Fig. 16h; Pearce, 2008). The samples derived from the blocks of N-MORB-, SSZ- and OIB-like oceanic basalts in the Ankara Mélange typically plot within the MORB-OIB mantle array (Fig. 16h).

The primitive mantle-normalized, multi-element diagrams of the representative samples from the high-K shoshonitic arc rocks around Kalecik (Ankara), Yapraklı (Çankırı) and Laloğlu (Çorum) are plotted in Fig. 17a. The trace element patterns of all the analyzed alkaline rocks display strong enrichment of the LILE, LREE and also Pb, U in

SED
5, 1941–2004, 2013

comparison to HFSE (Nb, Ta, Zr, Hf, Ti, Y), which show negative anomalies indicating subduction zone influence (Kempton et al., 1991). The high Ba/Ta (> 450) and Ba/Nb (> 28) ratios are characteristic features of subduction-related magmas (Fitton et al., 1988). The very high ratios of Ba/Ta (383–5255), Ba/Nb (64–538), and relatively high Zr/Nb (5–22), Th/Yb (2–14), Zr/Y (3–7) and La/Yb (9–36) have been attributed to a mantle source, which was enriched by a subduction component (Frey et al., 1978; Fitton et al., 1998; Maury et al., 1992; Schiano et al., 1995). However, some of the lamprophyre dike samples (DM.2, DM.6, DM.8, DM.9, DM.10) contain La/Yb ratios of 30, indicating highly undersaturated magmas for their origin. Also, the alkaline rocks with Mg # < 61, except for one sample (Mg# = 71), [MgO/(MgO × 0.8 + FeO total)], imply that none of these shoshonitic rocks represents primary mantle-derived subduction-related magmas. However, their chondrite-normalized REE patterns (Fig. 17b) show LREE enrichment, flat HREE ($La/Sm_n = 2.18–5.71$; $Gd/Lu_n = 1.69–4.14$; $La/Lu_n = 6.57–24.72$), and minor negative Eu anomalies ($Eu/Eu^* = 0.77–0.95$). These geochemical characteristics are compatible with those defining subduction-related, arc volcanic assemblages (Tatsumi et al., 1986; Kelemen et al., 1993; Hawkesworth et al., 1993; Pearce and Peate, 1995).

The high-K shoshonitic lamprophyric dikes are characterized by intermediate $^{143}Nd/^{144}Nd$ (0.512674–0.512690) and $^{87}Sr/^{86}Sr$ (0.704697–0.704892) isotopic compositions. The initial ε_{Nd} values range from +1.3 to +1.7, whereas the modern ε_{Nd} values vary between +0.7 and +1.0 indicating a relatively enriched mantle source. Their Pb isotope ratios range from 19.332 to 19.939 for $^{206}Pb/^{204}Pb$, 15.655 to 15.691 for $^{207}Pb/^{204}Pb$, and 39.192 to 39.612 for $^{208}Pb/^{204}Pb$. The high $^{206}Pb/^{204}Pb$, and relatively high $^{143}Nd/^{144}Nd$ and $^{87}Sr/^{86}Sr$ ratios seem to be compatible with a mantle source that is enriched by slab-derived fluids and/or subducted pelagic sediments.

SED
5, 1941–2004, 2013

7 Discussion

7.1 Source characteristics

The subduction-accretion complex represented by the Ankara Mélange contains blocks of oceanic lithosphere showing geochemical affinities ranging from MORB to IAT and calc-alkaline. The SSZ-type ophiolite assemblages in the melange display both IAT-like and boninitic geochemical signatures. The ophiolitic units with an IAT-like chemistry are the manifestation of partial melting of the upper mantle peridotites, which were modified by incompatible element-enriched hydrous fluids (or melt) released from the subducting Tethyan oceanic slab. The ophiolitic units with MORB-like signatures represent the products of a depleted mantle source. Some of the samples with MORB-like chemistry plot within or near the IAT field (Figs. 13c and 16h) indicating that their magmas were influenced by subduction-derived fluids. These ophiolitic rocks are the oldest units as constrained by the volcanic stratigraphy and crosscutting relationships. Some doleritic dikes and basaltic rocks in the ophiolites show boninitic affinities, consistent with their formation in a forearc setting (Dilek and Furnes, 2011; Sarifakioglu et al., 2011). Collectively, the ophiolitic units in the Ankara Mélange display a geochemical progression that is typical of the development of forearc oceanic crust in the early stages of subduction-induced magmatism, as also documented from other Tethyan ophiolites (Dilek and Furnes, 2009, 2011; Dilek and Thy, 2009; Pearce and Robinson, 2010; Saccani et al., 2011; Moghadam et al., 2013).

Seamount volcanic rocks occurring in the Ankara Mélange have OIB-like geochemical features, showing tholeiitic to alkaline affinities (Fig. 13e) with enrichment in incompatible elements and LREEs. The tholeiitic OIB affinity of some of the seamount volcanic rocks may have resulted from the interaction of plume-derived melts with MORB-type melts near a seafloor spreading system. The depletion of the OIB-type volcanic rocks in immobile elements (especially Ti) suggests mixing of the plume and MORB-type melts during seamount evolution.

SED
5, 1941–2004, 2013

The high-K alkaline rocks exhibit LILE and HFSE enrichments and negative Nb, Ta, Hf, Zr, Ti anomalies, indicating strong subduction influence in their melt evolution (Fig. 17a). The high ratios of LILE/HFSE (Ba/Nb = 64–538; Ba/Ta = 383–5255; Rb/Nb = ~2–20), LREE/HFSE (La/Nb = 1.8–7.2; La/Ta = 48–188; La/Sm_n ~4), LILE/LREE (Th/La = 0.16–0.49) and Zr/Nb (5–22), and the large negative Nb–Ta anomaly in the multi-element diagrams all point to a melt source affected by subduction-generated fluids and/or crustally contaminated magmas. The observed high Ba/Nb (64–538), La/Yb (9–36), Sr/Nd (14–45) and Ce/Yb (20–73) ratios, and low Nb/U (2–7), Ba/La (20.02–59.83), U/Th (0.13–0.50) and Ce/Pb (~2–20) values indicate that the mantle melt source may have been modified by some melts derived from relatively incompatible element-rich, subducted pelagic and/or terrigenous sediments. In contrast, the high Ce/Pb (25 + 5) and Nb/U (47+10) ratios observed in the OIB-type seamount volcanic rocks indicate that the magmas of these rocks were not modified by subducted sediments (Hoffman et al., 1986).

Enrichments in Cs, Rb, Ba, Th, U, K, La, Ce and Pb of the alkaline rocks suggest that their melt source was modified by subducted slab metarial (mainly fluids, and pelagic and/or terrigenous sediments). Slab-derived fluids helped to form hydrous and K-rich minerals, such as amphibole, apatite and phlogopite with high Rb/Sr (0.04–0.71) and K/Ti (3.77–16.62) ratios relative to MORB- and OIB-like magmas, and resulted in a positive correlation between Ba/Nb and La/Nb ratios (Fig. 18a). Also, the high La (18.4–69.2 ppm) contents and La/Yb ratios (9.5–34.6) reflect that the high-K magmas may have been produced by small degrees of partial melting of a subduction-metasomatised mantle source (Fig. 18b).

As illustrated in the $^{143}Nd/^{144}Nd$ vs. $^{87}Sr/^{86}Sr$ diagram (Fig. 19a), six lamprophyre samples plot on the mantle array defining a subduction component during the evolution of their magmas. We also show in this diagram, for comparison, the Late Cretaceous–Early Tertiary volcanic rocks from the southern part of Central Anatolia and the Eastern Pontides, and the Cenozoic volcanic units in Western Anatolia (Alpaslan et al., 2004, 2006; Eyüpoğlu, 2010; Altunkaynak and Dilek, 2006 and references therein).

SED
5, 1941–2004, 2013

The relatively high Pb (up to 34 ppm in some samples) and $^{87}Sr/^{86}Sr$ contents, and the Rb/Sr ratios (0.02–0.71) of the lamprophyre rocks also indicate the effects of subducted oceanic sediments added to the mantle melt source (Pearce and Peate, 1995). In the $^{206}Pb/^{204}Pb$ vs. $^{208}Pb/^{204}Pb$, $^{206}Pb/^{204}Pb$ vs. $^{207}Pb/^{204}Pb$, $^{87}Sr/^{86}Sr$ vs. $^{206}Pb/^{204}Pb$ and $^{143}Nd/^{144}Nd$ vs. $^{206}Pb/^{204}Pb$ variation diagrams, the data points lie above the Northern Hemisphere Reference Line (NHRL), and the radiogenic isotope data fall close to the fields of MORB, EMII and oceanic sediments. These features collectively suggest that the magmas of the lamprophyre rocks were derived from a MORB-like mantle source that was enriched by subducted terrigenous and carbonate sediments (Fig. 19b–e). However, the post-collisional Late Cretaceouse–Early Tertiary volcanic rocks in the Ulukisla basin in the southern part of Central Anatolia have higher $^{87}Sr/^{86}Sr$ and lower $^{143}Nd/^{144}Nd$ ratios than those of the lamprophyres in the Ankara Mélange, indicating an enriched lithospheric mantle source (EMII) with recycled, continent-derived material. The Late Cretaceous high-K volcanic rocks representing active continental margin arc units in the Eastern Pontides with low $^{87}Sr/^{86}Sr$ reflect a mantle source enriched by continental crustal rocks. The $^{143}Nd/^{144}Nd$, $^{87}Sr/^{86}Sr$, $^{206}Pb/^{204}Pb$, $^{208}Pb/^{204}Pb$ and $^{207}Pb/^{204}Pb$ values reflecting subduction enrichment and crustal contamination of the source of the post-collisional, Middle Eocene volcanic units in Central Anatolia and the Tertiary volcanic suites in western Anatolia have been explained by slab breakoff-induced asthenospheric upwelling and associated partial melting of the orogenic lithospheric mantle (Alpaslan et al., 2004, 2006; Altunkaynak and Dilek, 2006, 2013; Dilek and Altunkaynak, 2007; Keskin et al., 2008; Gündoğdu–Atakay, 2009; Sarifakioglu et al., 2013).

The depletion of HFSE elements with respect to LREE enrichment, and high LILE/HFSE and radiogenic isotope ratios suggest that the high-K shoshonitic rocks are likely to have formed by small degrees of partial melting of a lithospheric mantle modified by slab-derived hydrous fluids.

SED
5, 1941–2004, 2013

7.2 Tectonic model

The Ankara Mélange displays a heterogeneous structural architecture containing oceanic and crustal rocks with different internal structure, stratigraphy and geochemical compositions. The oldest ophiolitic rocks in the Ankara Mélange appear to have formed in a SSZ setting within the Northern Tethys around 180 Ma (Dilek and Thy, 2006; Sarifakioglu et al., 2011). The ~80 Ma (80.3 ± 7.6 Ma) ophiolitic rocks in the same mélange also indicate that oceanic crust formation in the Northern Tethys was still in operation in the Late Cretaceous (Table 1).

We obtained Middle–Upper Triassic biostratigraphic age data from the neritic limestones that are spatially associated with the seamount volcanic rocks, indicating that an oceanic lithosphere of the Late Triassic and older ages must have existed in this ocean to make up the substratum of the seamounts. Thus, we know that the northern branch of Neotethys was already a wide-open ocean with its MORB-type oceanic lithosphere between the Pontide block to the north and the Anatolide–Tauride microcontinent to the south in the Early Triassic (or even before). The ophiolitic mélange units in the Kırıkkale–Ankara–Çankırı–Çorum area are uncomformably overlain by basal volcanic conglomerates of an arc origin. The overlying volcanosedimentary units contain clayey- and sandy-limestone, limey sandstone, and sandstone-claystone alternating with volcaniclastic rocks. These rock types and their internal stratigraphy suggest their deposition in a frontal arc-forearc basin. The clayey limestones are intruded by dikes and sills and have Late Santonian, and Campanian–Maastrichtian ages based on their fossil contents (Sarifakioglu, unpublished data). The radiometric age data from an alkaline basaltic rock (YK.4) and a syeno-diorite intrusion (YK.438) give ages of 67.8 ± 4.9 Ma and 75.9 ± 1.3 Ma, respectively (Table 4a and d), constraining the timing of intra-oceanic arc magmatism as the Latest Cretaceous.

In general, subalkaline (tholeiitic and calcalkaline) volcanic arc rocks occur in the northern part of the study area, whereas the younger alkaline volcanic and plutonic rocks in the south. We interpret this spatial and temporal relationship to have resulted

SED
5, 1941–2004, 2013

from a southward progression of the arc magmatism from subalkaline to alkaline affinities through time due to arc rifting above the southward retreating Tethyan subduction system (Fig. 20). We, therefore, think that the arc-related late alkaline dikes and plutons were emplaced on and across the evolving subduction-accretion complex above the north-dipping, southward rolling Tethyan slab.

The high-K and shoshonitic Eocene dikes and lavas in the Ankara Mélange formed from melts derived from partial melting of the metasomatized arc mantle that was triggered by the influx of slab breakoff-induced asthenospheric flow.This slab breakoff was a result of an arc-continent (Central Anatolian Crystalline Complex – CACC) collision, followed by the continent-continent collision (Sakarya and CACC) in the Early to Middle Eocene.

8 Conclusions

1. Blocks of Middle–Late Triassic seamount and Upper Permian metamorphic rocks occurring in the Ankara Mélange represent an intra-oceanic subduction-accretion complex that developed in the Northern Tethys during the Late Paleozoic through Cretaceous.

2. Thrust sheets and/or megablocks containing SSZ ophiolite units with Liassic and Cretaceous ages were incorporated into this subduction-accretion complex during the Early Late Cretaceous.

3. The Late Cretaceous tholeiitic to calc-alkaline volcanic rocks are the products of an intra-oceanic island arc system. The tholeiitic and calc-alkaline arc rocks shown enrichment in incompatible elements due to the influence of slab-derived fluids. The shoshonitic arc rocks representing the latest stage of island arc magmatism were produced by partial melting of a subduction-enriched mantle source.

SED
5, 1941–2004, 2013

Acknowledgements. This study was suppoted by a grant from the General Directorate of Mineral Research and Exploration of Turkey (MTA, Ankara; Project no: 2007–2008.30.1601.d-f). We thank Yakov Kapusta (ACTLabs, Canada) for the radiometric and isotopic analyses of our rock samples in a timely fashion, and for his help with the interpretation of the obtained data. Special thanks are due to Francesca Funiciello for her editorial suggestions, which improved the manuscript. We would like to acknowledge the Head of the Geological Research Department, Erol Timur, in MTA-Ankara for his continued support of our *Ophiolite Inventory Project* in Turkey over the last two years.

References

Akyürek, B., Bilginer, E., Akbaş, B., Hepşen, N., Pehlivan, Ş., Sunu, O., Soysal, T., Dağer, Z., Çatal, E., Sözeri, B., Yıldırım, H., and Hakyemez, Y.: Fundamental geological characteristics of Ankara-Elmadag-Kalecik area, Journal of Geological Engineering (Jeoloji Mühendisligi Dergisi), Chamber of Geological Engineers of Turkey (TMMOB Jeoloji Mühendisleri Odasi), 20, 31–46, 1984 (in Turkish with English abstract).

Alpaslan, M., Frei, R., Boztug, D., Kurt, M. A., and Temel, A.: Geochemical and Pb–Sr–Nd isotopic constraints indicating an enriched-mantle source for Late Cretaceous to Early Tertiary volcanism, Central Anatolia, Turkey, Int. Geol. Rev., 46, 1023–1041, 2004.

Alpaslan, M., Boztug, D., Frei, R., Temel, A, and Kurt, M. A.: Geochemical and Pb–Sr–Nd isotopic composition of the ultrapotassic volcanic rocks from the extension-related Çamardı–Ulukisla basin, Nigde Province, Central Anatolia, Turkey, J. Asian Earth Sci., 27, 613–627, 2006.

Altunkaynak, Ş. and Dilek, Y.: Timing and nature of postcollisional volcanism in Western Anatolia and geodynamic implications, in: Postcollisional Tectonics and Magmatism in the Mediterranean Region and Asia, edited by: Dilek, Y. and Pavlides, S., Geol. S. Am. S., 409, 321–351, 2006.

Altunkaynak, Ş. and Dilek, Y.: Eocene mafic volcanism in northern Anatolia: its causes and mantle sources in the absence of active subduction, Int. Geol. Rev., 55, 1641–1659, 2013.

Bailey, E. B. and McCallien, W. S.: The Ankara Mélange in Central Anatolia, Bulletin of the Mineral Research and Exploration Institute of Turkey, Maden Tetkik ve Arama Enstitüsú, Ankara, Turkey, 40, 12–22, 1950.

SED

5, 1941–2004, 2013

Bailey, E. B. and McCallien, W. S.: The Ankara Mélange and Anatolia Thrust, Nature, 166, 938–941, 1953.
Bingöl, E., Akyürek, B., and Korkmazer, B.: Geology of Biga Peninsula and characteristics of Karakaya formation, in: Geoscience Congress of 50th Anniversary of the Turkish Republic, Ankara, 1975, the Publications of MTA General Directorate, 70–77, 1975 (in Turkish with English abstract).
Boztug, D.: S–I–A type intrusive associations: geodynamic significance of synchronism between metamorphism and magmatism in Central Anatolia, Turkey, in: Tectonics and Magmatism in Turkey and the Surrounding Area, edited by: Bozkurt, E., Winchester, J. A., and Piper, J. D. A., Geological Society of London Special Publication, 173, 441–458, 2000.
Çoğulu, E., Delaloye, M., and Chessex, R.: Sur l'age de quelques roches plutoniques acides dans region d'Eskişehir, Turquie, Archives des Sciences, Genève, 18, 692–699, 1965.
Cox, K. G., Bell, J. D., and Pankhurst, R. J.: The Interpretation of Ignous Rocks, Allen and Unwin, London, 450 pp., 1979.
Dangerfield, A., Harris, R. Sarifakioglu, E., and Dilek, Y.: Tectonic evolution of the Ankara Mélange and associated Eldivan ophiolite near Hançili, Central Turkey, Geol. S. Am. S., 480, 143–169, 2011.
Delaloye, M. and Bingöl, E.: Granitoids from western and Northwestern Anatolia: geochemistry and modelling of geodynamic evolution, Int. Geol. Rev., 42, 241–268, doi:10.1080/00206810009465081, 2000.
Dilek, Y. and Altunkaynak, Ş.: Cenozoic crustal evolution and mantle dynamics of post–collisional magmatism in Western Anatolia, Int. Geol. Rev., 49, 431–453, 2007.
Dilek, Y. and Furnes, H.: Structure and geochemistry of Tethyan ophiolites and their petrogenesis in subduction rollback systems, Lithos, 113, 1–20, 2009.
Dilek, Y. and Furnes, H.: Ophiolite genesis and global tectonics: geochemical and tectonic fingerprinting of ancient oceanic lithosphere, Geol. Soc. Am. Bull., 123, 387–411, doi:10.1130/B30446.1, 2011.
Dilek, Y. and Thy, P.: Age and petrogenesis of plagiogranite intrusions in the Ankara Mélange, Central Turkey, Isl. Arc, 15, 44–57, 2006.
Dilek, Y. and Thy, P.: Island arc tholeiite to boninitic melt evolution of the Cretaceous Kizildag (Turkey) ophiolite: model for multi-stage early arc-forearc magmatism in Tethyan subduction factories, Lithos, 113, 68–87, 2009.

SED
5, 1941–2004, 2013

Dönmez, M., Akçay, A. E., Türkecan, A., Evcimen, Ö., Atakay, E., and Görmüş, T.: Tertiary volcanites in Ankara surroundings, Mineral Research and Exploration Institute of Turkey (MTA) Report, No. 11164, 116 pp., Ankara, Turkey, 2009 (in Turkish, unpublished).
Eyüpoğlu, Y.: Late cretaceous high-K volcanism in the eastern pontide orogenic belt: implications for the geodynamic evolution of NE Turkey, Int. Geol. Rev., 52, 142–186, 2010.
Fitton, J. G., James, D., Kempton, P. D., Ormerod, D. S., and Leeman, W. P.: The role of lithospheric mantle in the generation of Late Cenozoic basic magmas in the Western United States, J. Petrol., Special Lithosphere Issue, 331–349, 1988.
Frey, F. A., Green, D. H., and Roy, S. D.: Integrated models of basalt petrogenesis: a study of quartz tholeiite to olivine melililites from Southeastern Australia utilizing geochemical and experimental data, J. Petrol., 19, 463–513, 1978.
Güleç, N.: Rb–Sr isotope data from the Agacoren granitoid (east of Tuz Gölü): geochronological and genetical implications, Turk. J. Earth Sci., 3, 39–43, 1994.
Gündoğdu-Atakay, E.: Geological and petrological characteristics of volcanic rocks at soutwest of Çorum and geoarcheological studies at Alaca höyük excavation site, PhD Thesis, Ankara University, Ankara, Turkey, 194 pp., 2009.
Hakyemez, Y., Barkurt, M. Y., Bilginer, E., Pehlivan, Ş., Can, B., Dağer, Z., and Sözeri, B.: The geology of Yapraklı–Ilgaz–Çankırı–Çandır surroundings, Mineral Research and Exploration Institute of Turkey (MTA) Report, No. 7966, Ankara, Turkey, 1986 (in Turkish, unpublished).
Hastie, A. R., Kerr, A. C., Pearce, J. A., and Mitchell, S. F.: Classification of altered volcanic island arc rocks using immobile trace elements: development of the Th–Co discrimination diagram, J. Petrol., 48, 2341–2357, 2007.
Hawkesworth, C. J., Gallagher, K., Hergt, J. M., and McDermott, F.: Mantle and slab contributions in arc magmas, Annu. Rev. Earth Pl. Sc., 21, 175–204, 1993.
Hoffman, A. W., Jochum, K. P., Seufert, M., and White, W. M.: Nb and Pb in oceanic basalts: new constraints on mantle evolution, Earth Planet. Sc. Lett., 90, 421–436, 1986.
Ilbeyli, N., Pearce, J. A., Thirwall, M. F., and Mitchell, J. G.: Petrogenesis of collision-related plutonics in Central Anatolia, Turkey, Lithos, 72, 163–182, 2004.
Irvine, T. N. and Baragar, W. R. A.: A guide to the chemical classification of the common volcanic rocks, Canadian Journal of Earth Sciences, 8, 523–548, doi:10.1139/e71-055, 1971.
Kadıoglu, Y. K., Dilek, Y., Güleç, N., and Foland, K. A.: Tectonomagmatic evolution of bimodal plutons in the Central Anatolian Crystalline Complex, Turkey, J. Geol., 111, 671–690, 2003.

SED
5, 1941–2004, 2013

Kadıoglu, Y. K., Dilek, Y., and Foland, K. A.: Slab breakoff and syncollisional origin of the Late Cretaceous magmatism in the Central Anatolian Crystalline Complex, Turkey, in: Postcollisional Tectonics and Magmatism in the Mediterranean Region and Asia, edited by: Dilek, Y. and Pavlides, S., Geol. S. Am. S., 409, 381–415, doi:10.1130/2006/2409(19), 2006.
Kelemen, P. B., Shimizu, N., and Dunn, T.: Relative depletion of niobium in some arc magmas and the continental crust: partitioning of K, Nb, La and Ce during melt/rock reaction in the upper mantle, Earth Planet. Sc. Lett., 120, 111–134, 1993.
Kempton, P. D., Fitton, J. G., Hawkesworth, C. J., and Ormerod, D. S.: Isotopic and trace element contraints on the composition and evolution of the lithosphere beneath the Southern United State, J. Geophys. Res., 96, 13713–13735, 1991.
Keskin, M., Genç, C.Ş and Tüysüz, O.: Petrology and geochemistry of post-collisional Middle Eocene volcanic units in North-Central Turkey: evidence for magma generation by slab breakoff following the closure of the Northern Noetethys Ocean, Lithos, 104, 267–305, 2008.
Koçyiğit, A.: An example of an accretionary forearc basin from northern Central Anatolia and its implications for the history of the Neo-Tethys in Turkey, Geol. S. Am. S., 103, 22–36, 1991.
Le Bas, M. J., Le Maitre, R. W., Streckeisen, A., and Zanettin, B.: Achemical classification of volcanic rocks based on total Alcali–Silica content, J. Petrol., 27, 745–750, 1986.
Maury, R. C., Defant, M. J., and Joron, J. L.: Metasomatism of arc mantle inferred from trace elements in Philippine xenoliths, Nature, 360, 661–663, doi:10.1038/360661a0, 1992.
Moghadam, H. S., Stern, R. J., Chiaradia, M., and Rahgoshay, M.: Geochemistry and tectonic evolution of the Late Cretaceous Gogher-Baft ophiolite, Central Iran, Lithos, 168, 33–47, doi:10.1016/j.lithos.2013.01.013, 2013.
MTA: The geological map of Turkey, 1/500 000 scaled, Geological Survey of Turkey, The General Directorate of Mineral Research and Exploration, Ankara, Turkey, 2001.
Muller, D., Rock, N. M. S., and Groves, D. I.: Geochemical discrimination between shoshonitic and potassic volcanic rocks in different tectonic settings: a pilot study, Miner. Petrol., 46, 259–289, 1992.
Norman, T. N.: The role of the Ankara Melange in the development of Anatolia (Turkey), in: The Geological Evolution of the Eastern Mediterranean, edited by: Dixon, J. E., and Robertson, A. H. F., Geological Society of London Special Publication, 17, 441–447, 1984.
Nzegge, O. M., Satır, M., Siebel, W., and Taubald, H.: Geochemical and isotopic constraints on the genesis of the Late Palaeozoic Deliktaş and Sivrikaya granites from the Kastamonu granitoid belt (Central Pontides, Turkey), Neues Jb. Miner. Abh., 183, 27–40, 2006.

SED
5, 1941–2004, 2013

Okay, A. I. and Göncüoğlu, M. C.: Karakaya complex: a review of data and concepts, Turk. J. Earth Sci., 13, 77–95, 2004.
Okay, A. I., Monod, O., and Monié, P.: Triassic blueschists and eclogites from Northwest Turkey: vestiges of the Paleo-Tethyan subduction, Lithos, 64, 155–178, 2002.
Okay, A. I., Tüysüz, O., Satır, M., Özkan-Altıner, S., Altıner, D., Sherlock, S., and Eren, R. H.: Cretaceous and Triassic subduction-accretion HP–LT metamorphism and continental growth in the Central Pontides, Turkey, Geol. Soc. Am. Bull., 118, 1247–1269, doi:10.1130/B25938.1, 2006.
Pearce, J. A.: Trace element characteristics of lavas from destructive plate boundaries, in: Andesites: Orogenic Andesites and Related Rocks, edited by: Thorpe, R. S., John Wiley & Sons, Chichester, 525–548, 1982.
Pearce, J. A.: Geochemical fingerprinting of oceanic basalts with applications to ophiolite classification and the search for Archean oceanic crust, Lithos, 100, 14–48, 2008.
Pearce, J. A. and Cann, J. R.: Tectonic setting of basic volcanic rocks determined using trace element analyses, Earth Planet. Sc. Lett., 19, 290–300, 1973.
Pearce, J. A. and Peate, D. W.: Tectonic implications of the composition of volcanic arc magmas, Annu. Rev. Earth Pl. Sc., 23, 251–285, doi:10.1146/annurev.ea.23.050195.001343, 1995.
Pearce, J. A. and Robinson, P. T.: The Troodos ophiolitic complex probably formed in a subduction initiation, slab edge setting, Gondwana Res., 18, 60–81, doi:10.1016/j.gr.2009.12.003, 2010.
Pearce, J. A., Harris, B. W., and Tindle, A. G.: Trace element discrimination diagrams for the tectonic interpretation of granitic rocks, J. Petrol., 25, 956–983, 1984.
Peccerillo, A. and Taylor, S. R.: Geochemistry of Eocene calc-alkaline volcanic rocks from the Kastamonu area, Northern Turkey, Contrib. Mineral. Petr., 58, 63–81, 1976.
Plechov, P. Y., Tsai, A. E., Shcherbakov, V. D., and Dirksen, O. V.: Opacitization conditions of hornblende in Bezymyannyi volcano andesites (30 March 1956 eruption), Petrology, 1, 19–35, 2008.
Rojay, B. and Süzen, L.: Tectonostratigraphic evolution of the Cretaceous dynamic basins on accretionary ophiolitic melange prism, SW of Ankara Region, Turkish Association of Petroleum Geologists Bulletin, 9, 1–12, 1997.
Rojay, B., Altıner, D., Altıner Özkan, S., Önen, A. P., James, S., and Thirlwall, M. F.: Geodynamic significance of the Cretaceous pillow basalts from North Anatolian Ophiolitic Mélange

SED
5, 1941–2004, 2013

(Central Anatolia, Turkey): geochemical and paleontological constraints, Geodin. Acta, 17, 349–361, 2004.
Saccani, E., Beccaluva, L., Photiades, A., and Zeda, O.: Petrogenesis and tectono-magmatic significance of basalts and mantle peridotites from the Albanian–Greek ophiolites and sub-ophiolitic mélanges. New constraints for the Triassic–Jurassic evolution of the Neo-tethys in the Dinaride sector, Lithos, 124, 227–242, 2011.
Sarıfakıoğlu, E., Dilek, Y., and Winchester, J. A.: Late Cretaceous subduction initiation and Paleocene–Eocene slab breakoff magmatism in South-Central Anatolia, Turkey, Int. Geol. Rev., 55, 66–87, 2013.
Sarifakioglu, E., Sevin, M., Esirtgen, E., Bilgiç, T., Duran, S., Parlak, O., Karabalık, N., Alemdar, S., Dilek, Y., and Uysal, İ.: The geology of ophiolitic rocks around Çankırı–Çorum Basen: petrogenesis, tectonics and ore deposits, Mineral Research and Exploration Institute of Turkey (MTA) Report, No. 11449, 196 pp., 2011 (in Turkish, unpublished),
Schiano, P., Clocchiatti, R., Shimizu, N., Mury, R. C., Johum, K. P., and Hofmann, A. W.: Hydrous, silica rich melts in the subarc mantle and their relationship with erupted arc lavas, Nature, 377, 595–600, doi:10.1038/377595a0, 1995.
Shand, S. J.: Eruptive Rocks, Thomas Murby & Co., London, 1–360, 1927.
Shervais, J. W.: Ti–V plots and the petrogenesis of modern and ophiolitic lavas, Earth Planet. Sc. Lett., 59, 101–118, 1982.
Sun, S. S. and McDonough, W. F.: Chemical and isotopic systematics of oceanic basalts: implications for mantle composition and processes, in: Magmatism in the Ocean Basins, edited by: Saunders, A. D. and Norry, M. J., Geol. Soc. Spec. Publ., 42, 313–345, 1989.
Tankut, A., Dilek, Y., and Önen, P.: Petrology and geochemistry of the Neo–Tethyan volcanism as revealed in the Ankara melange, Turkey, J. Volcanol. Geoth. Res., 85, 265–284, 1998.
Tatsumi, Y., Hamilton, D., and Nesbitt, R. W.: Chemical characteristics of fluid phase released from a subducted lithosphere and origin of arc magmas. Evidence from high pressure experiments and natural rocks, J. Volcanol. Geoth. Res., 29, 293–309, 1986.
Tekeli, O.: Subduction complex of pre–Jurassic age, Northern Anatolia, Turkey, Geology, 9, 68–72, 1981.
Topuz, G., Altherr, R., Satır, M., and Schwarz, M.: Low grade metamorphic rocks from the Pulur complex, NE Turkey: implications for pre–Liassic evolution of the Eastern Pontides, Int. J. Earth Sci., 93, 72–91, doi:10.1007/s00531-003-0372-5, 2004.

SED
5, 1941–2004, 2013

Topuz, G., Okay, A. I., Altherr, R., Meyer, H. P., and Nasdala, L.: Partial high-pressure aragonitization of micritic limestones in an accretionary complex, Tavşanlı Zone, NW Turkey, J. Metamorph. Geol., 24, 603–613, 2006.
Tüysüz, O., Dellaloğlu, A. A., and Terzioğlu, N.: A magmatic belt within the Neo-tethyan suture zone and its role in the tectonic evolution of Northern Turkey, Tectonophysics, 243, 173–191, 1995.
Uğuz, M. F., Sevin, M., and Duru, M.: 1/500 000 Scale Geological Maps of Turkey, Sinop Quadrangle, MTA General Directorate, Ankara, 2002.
White, W. M.: Sources of oceanic basalts: radiogenic isotopic evidence, Geology, 13, 115–118, 1985.
Whitney, D. L. and Dilek, Y.: Metamorphism during crustal thickening and extension in Central Anatolia: the Nigde metamorphic core complex, J. Petrol., 39, 1385–1403, 1998.
Wood, D. A.: The application of a Th–Hf–Ta diagram to problems of tectonomagmatic classification and to establishing the nature of crustal contamination of basaltic lavas of the British Tertiary Volcanic Province, Earth Planet. Sc. Lett., 56, 11–30, 1980.
Zindler, A. and Hart, S. R.: Chemical geodynamics, Annu. Rev. Earth Pl. Sc., 14, 493–571, 1986.

SED
5, 1941–2004, 2013

Table 1. Whole-rock $^{40}Ar/^{39}Ar$ age data for a basaltic rock sample (YK-11) from the youngest SSZ ophiolite in the Ankara Mélange, Turkey.

Sample: YK-11 (whole rock): Basalt, $J = 0.004426 \pm 0.000051$

T °C	^{40}Ar cc(STP)	$^{40}Ar/^{39}Ar$	±1σ	$^{38}Ar/^{39}Ar$	±1σ	$^{37}Ar/^{39}Ar$	±1σ	$^{36}Ar/^{39}Ar$	±1σ	Ca/K	$\sum^{39}Ar$ (%)	Age (Ma) ±1σ	±1σ
500	20.81×10^{-9}	29.6	0.1	0.0418	0.0029	0.479	0.011	0.0620	0.0049	1.72	40.5	88.0	11.0
600	9.45×10^{-9}	22.5	0.1	0.0364	0.0037	0.584	0.011	0.0438	0.0033	2.10	64.8	74.4	7.6
700	12.18×10^{-9}	79.8	0.6	0.0733	0.0129	0.627	0.036	0.2306	0.0075	2.26	73.6	90.6	16.5
800	9.18×10^{-9}	184.7	9.4	0.1457	0.0530	0.751	0.145	0.5966	0.0347	2.70	76.5	65.7	38.7
1000	9.00×10^{-9}	58.5	0.7	0.0714	0.0153	1.630	0.046	0.1440	0.0125	5.87	85.3	123.2	27.4
1130	8.12×10^{-9}	32.0	0.2	0.0332	0.0070	1.131	0.019	0.0811	0.0055	4.07	100.0	62.9	12.6

Age spectrum: the sample yielded age spectrum with well behaved plateau, characterized by 73.6 % of ^{39}Ar, Age value of 80.3 ± 7.6 Ma.
On the inverse isochrone plot points form linear regression characterized by age value of 75.8 ± 7.4 and $(^{40}Ar/^{36}Ar)_0 = 300 \pm 8$.

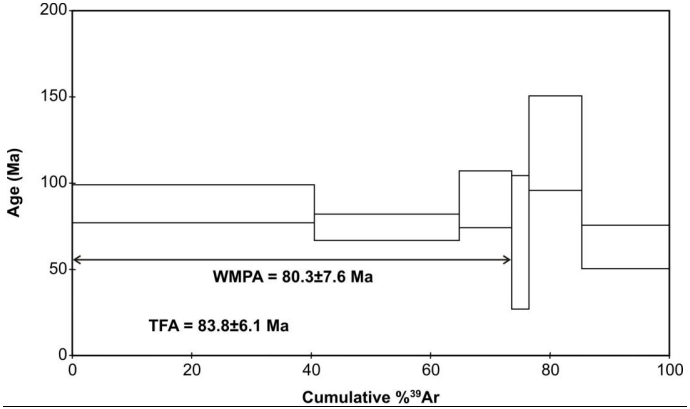

SED
5, 1941–2004, 2013

Table 2a. Whole-rock $^{40}Ar/^{39}Ar$ age data for an epidote-glaucophane schist rock from a metamorphic block in the Ankara Mélange, Turkey.

Sample: YK-6: epidote-glaucophane schist, $J = 0.004420 \pm 0.000051$

T °C	^{40}Ar cc (STP)	$^{40}Ar/^{39}Ar$	±1σ	$^{38}Ar/^{39}Ar$	±1σ	$^{37}Ar/^{39}Ar$	±1σ	$^{36}Ar/^{39}Ar$	±1σ	Ca/K	$\sum^{39}Ar$ (%)	Age (Ma) ±1σ	±1σ
500	35.70×10^{-9}	48.05	0.1	0.0463	0.003	1.5385	0.0082	0.1299	0.002	5.54	6.4	75.4	4.6
600	32.83×10^{-9}	18.75	0.02	0.0257	0.0005	1.221	0.0031	0.0274	0.0012	4.4	21.5	83.1	2.9
700	38.21×10^{-9}	17.65	0.01	0.0255	0.0007	0.5962	0.0014	0.0229	0.0006	2.15	40.1	**84.7**	**1.7**
800	40.74×10^{-9}	19.89	0.02	0.0236	0.001	1.3996	0.0017	0.027	0.0008	5.04	57.8	92.7	2.1
900	21.78×10^{-9}	19.32	0.03	0.0277	0.0008	10.821	0.0144	0.0325	0.0012	38.96	67.5	75.8	2.9
1000	16.15×10^{-9}	14.81	0.03	0.0253	0.0016	12.5237	0.0228	0.0168	0.0017	45.09	76.9	76.8	4
1130	35.36×10^{-9}	13.2	0.01	0.0244	0.0004	9.9743	0.0097	0.0145	0.0009	35.91	100	69.8	2.2

Age Spectrum: the sample yielded age spectrum with two 3 steps plateaus, characterized accordingly by 40.1 % of ^{39}Ar, Age value of 83.5 ± 1.7 Ma and 42.2 % of ^{39}Ar, Age value of 72.2 ± 2.2 Ma. On the Inverse Isochrone Plot points form two linear regression characterized by age value of 87.8 ± 2.5 and $(^{40}Ar/^{36}Ar)_0 = 285 \pm 5$. The presence of two age plateaus evidence to isotope heterogeneity of YK 6.

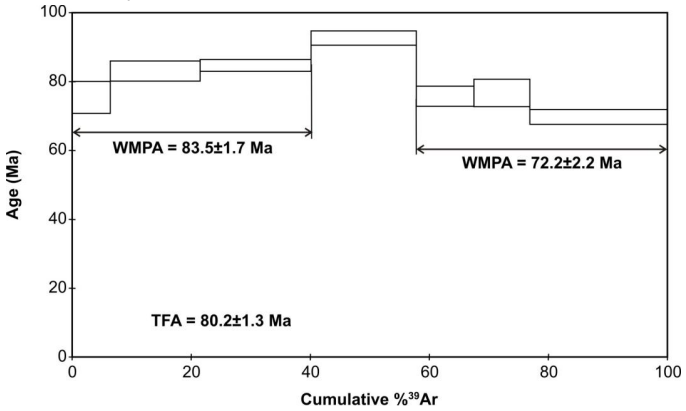

SED
5, 1941–2004, 2013

Table 2b. Whole-rock $^{40}Ar/^{39}Ar$ age data for an epidote-chlorite schist rock from a metamorphic block in the Ankara Mélange, Turkey.

Sample: YK-7: epidote-chlorite schist, $J = 0.004121 \pm 0.000044$

T °C	^{40}Ar cc (STP)	$^{40}Ar/^{39}Ar$	±1σ	$^{38}Ar/^{39}Ar$	±1σ	$^{37}Ar/^{39}Ar$	±1σ	$^{36}Ar/^{39}Ar$	±1σ	Ca/K	$\sum^{39}Ar$ (%)	Age (Ma) ±1σ	±1σ
500	33.53×10^{-9}	57.6	0.2	0.051	0.0027	4.4795	0.0134	0.1488	0.0027	16.13	16.1	98.8	5.7
600	31.15×10^{-9}	38.4	0.1	0.0304	0.0018	3.5391	0.0081	0.0525	0.0019	12.74	38.7	**162.5**	**4.2**
700	42.75×10^{-9}	44.5	0.1	0.0355	0.0018	5.4612	0.0142	0.0761	0.0023	19.66	65.3	156.8	4.9
800	19.66×10^{-9}	31	0.1	0.0271	0.0028	1.8875	0.0089	0.0323	0.0027	6.8	82.9	153.1	5.8
900	12.92×10^{-9}	50.5	0.4	0.0507	0.0062	3.436	0.0365	0.1139	0.0087	12.37	90	121	17.9
1000	6.24×10^{-9}	60.7	1	0.0518	0.0203	11.168	0.1806	0.1419	0.0162	40.2	92.8	134.7	32.7
1130	22.81×10^{-9}	88.4	0.5	0.0743	0.0064	56.2813	0.3389	0.2421	0.0062	202.61	100	121.4	12.4

Age Spectrum: The sample yielded age spectrum with 3 steps plateau, characterized by 66.7 % of ^{39}Ar, Age value of 158.4 ± 4.2 Ma. On the Inverse Isochrone Plot points form linear regression characterized by age value of 166.9 ± 5.9 and $(^{40}Ar/^{36}Ar)_0 = 272 \pm 8$.

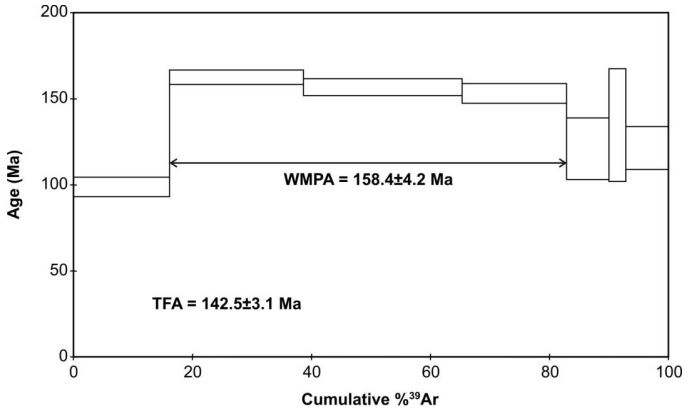

SED
5, 1941–2004, 2013

Table 2c. Whole-rock $^{40}Ar/^{39}Ar$ age data for an epidote-actinolite schist rock from a metamorphic block in the Ankara Mélange, Turkey.

Sample: YK-1: epidote-actinolite schist, $J = 0.004428 \pm 0.000051$

T °C	^{40}Ar cc (STP)	$^{40}Ar/^{39}Ar$	$\pm 1\sigma$	$^{38}Ar/^{39}Ar$	$\pm 1\sigma$	$^{37}Ar/^{39}Ar$	$\pm 1\sigma$	$^{36}Ar/^{39}Ar$	$\pm 1\sigma$	Ca/K	$\sum^{39}Ar$ (%)	Age (Ma) $\pm 1\sigma$	$\pm 1\sigma$
500	28.20×10^{-9}	195.111	1.614	0.1185	0.0072	8.7082	0.0754	0.5725	0.0095	31.35	4.1	196.1	17.7
600	35.22×10^{-9}	109.08	0.736	0.0809	0.0035	12.8319	0.0878	0.2835	0.007	46.19	13.2	191.6	14.5
700	46.14×10^{-9}	52.526	0.083	0.0345	0.0021	5.2249	0.0101	0.0848	0.0016	18.81	38.1	207	4
800	22.10×10^{-9}	43.305	0.132	0.032	0.0025	3.3143	0.0128	0.0652	0.003	11.93	52.5	182.5	6.8
900	28.97×10^{-9}	56.607	0.158	0.0384	0.0023	16.1294	0.0458	0.1083	0.0028	58.07	67	**186.6**	**6.3**
1000	30.80×10^{-9}	41.871	0.112	0.0328	0.0018	21.4028	0.0573	0.0558	0.0027	77.05	87.8	192.1	6
1130	30.24×10^{-9}	69.813	0.261	0.0523	0.0025	34.5698	0.1292	0.1345	0.0038	124.45	100	225.6	8.2

Age Spectrum: The sample yielded age spectrum with 3 steps plateau, characterized by 50 % of ^{39}Ar, Age value of 187.4 ± 3.7 Ma. On the Inverse Isochrone Plot one can observe linear regression characterized by age value of 166.1 ± 12.3.

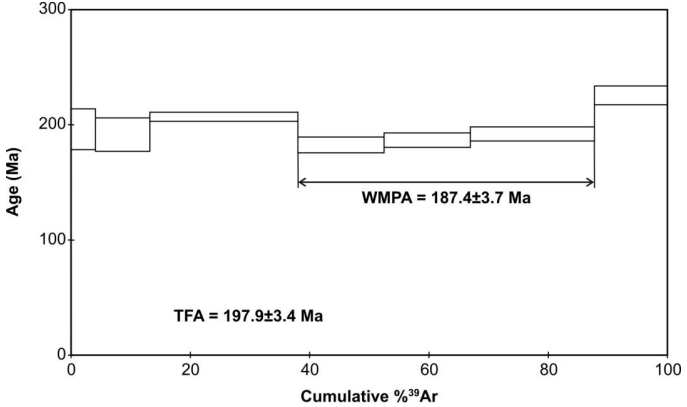

SED
5, 1941–2004, 2013

Table 3. Whole-rock K/Ar age data from metamorphic rock blocks in the Ankara Mélange, Turkey.

Sample no.	Rock	%K	$^{40}Ar/^{36}Ar$	$^{40}Ar_{rad}$, nl g^{-1}	% $^{40}Ar_{air}$	error	Age, Ma
CE.981	Phyllite	1.68	883.2	7.932	33.5	4.5	119.8 ± 3.3
CE.228	Actinolite schist	0.36	347.8	2.558	85.1	0.6	177.4 ± 5.8
CE.976	Amphibole-epidote schist	0.22	405.9	2.316	72.9	1.3	256.9 ± 8.0

SED
5, 1941–2004, 2013

Table 4a. Whole-rock $^{40}Ar/^{39}Ar$ age data for an island-arc basaltic rock (Sample No. YK-4) in the Ankara Mélange, Turkey.

Sample: YK-4 (whole rock): Basalt, $J = 0.004353 \pm 0.000050$

T °C	^{40}Ar cc (STP)	$^{40}Ar/^{39}Ar$	±1σ	$^{38}Ar/^{39}Ar$	±1σ	$^{37}Ar/^{39}Ar$	±1σ	$^{36}Ar/^{39}Ar$	±1σ	Ca/K	$\sum^{39}Ar$ (%)	Age (Ma)	±1σ
500	44.60×10^{-9}	168.69	0.97	0.1269	0.007	7.5932	0.0458	0.539	0.0065	27.34	6.9	72.4	12.8
600	14.83×10^{-9}	32.9	0.17	0.0413	0.0033	10.1845	0.0528	0.0795	0.0051	36.66	18.7	72.4	11.4
700	13.82×10^{-9}	26.82	0.1	0.0333	0.0048	4.2753	0.017	0.0621	0.0036	15.39	32.2	65.2	8
800	24.70×10^{-9}	26.65	0.08	0.0331	0.0022	1.935	0.0067	0.0635	0.0029	6.97	56.5	60.8	6.6
900	18.59×10^{-9}	18.29	0.04	0.021	0.0013	1.3887	0.0051	0.0299	0.0022	5	83.1	72.8	4.9
1000	7.83×10^{-9}	31.49	0.17	0.0381	0.0053	1.4804	0.0211	0.0611	0.0055	5.33	89.7	102.6	12.1
1130	11.68×10^{-9}	29.58	0.12	0.0279	0.0033	3.5167	0.016	0.054	0.0041	12.66	100	104	9.2

Age Spectrum: The sample yielded age spectrum with 3 steps plateau, characterized by 64.4 % of ^{39}Ar, Age value of 67.8 ± 4.9 Ma. On the Inverse Isochrone Plot points form linear regression characterized by age value of 68.1 ± 4.4 and $(^{40}Ar/^{36}Ar)_0 = 296.1 \pm 3.5$.

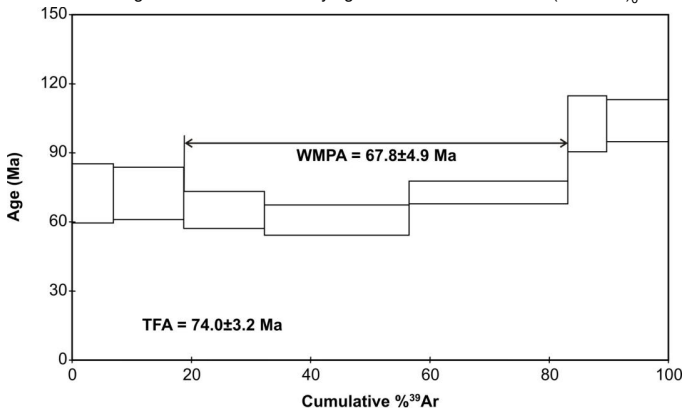

SED
5, 1941–2004, 2013

Table 4b. $^{40}Ar/^{39}Ar$ biotite age data for a lamprophyre dike (Sample No. YK-19) from the island-arc unit in the Ankara Mélange, Turkey.

Sample: YK-19 (biotite): Lamprophyre, $J = 0.007143 \pm 0.000133$

T °C	^{40}Ar cc (STP)	$^{40}Ar/^{39}Ar$	±1σ	$^{38}Ar/^{39}Ar$	±1σ	$^{37}Ar/^{39}Ar$	±1σ	$^{36}Ar/^{39}Ar$	±1σ	Ca/K	$\sum^{39}Ar$ (%)	Age (Ma) ±1σ	±1σ
500	3.9×10^{-9}	92.802	0.0393	0.015480	0.004274	0.61970	0.05770	0.028643	0.001314	22.30	0.6	10.50	5.0
625	7.7×10^{-9}	83.584	0.0116	0.015744	0.001217	0.31455	0.01480	0.015871	0.001284	1.13	2.0	46.7	4.80
750	37.9×10^{-9}	69.914	0.0044	0.013301	0.000117	0.05874	0.00360	0.008418	0.000210	0.21	10.40	57.1	1.30
850	45.7×10^{-9}	64.526	0.0017	0.013498	0.000076	0.04725	0.00102	0.004948	0.000237	0.17	21.20	63.2	1.40
950	51.6×10^{-9}	65.506	0.0033	0.013393	0.000248	0.08738	0.00394	0.004805	0.000142	0.31	33.3	64.9	1.30
1050	112.6×10^{-9}	62.462	0.0035	0.013738	0.000060	0.07037	0.00091	0.004305	0.000083	0.25	61.0	63.0	1.20
1130	156.9×10^{-9}	61.778	0.0020	0.013593	0.000030	0.07395	0.00067	0.003986	0.000051	0.27	100.0	63.3	1.20

Age Spectrum: The sample yielded age spectrum with four steps Plateau characterized by 89.6 % of ^{39}Ar, Age value of 63.6 ± 1.2 Ma. On the Inverse Isochrone Plot plateau points form linear trend, characterized by age value of 57.5 ± 4.1 Ma, MSWD = 1.5.

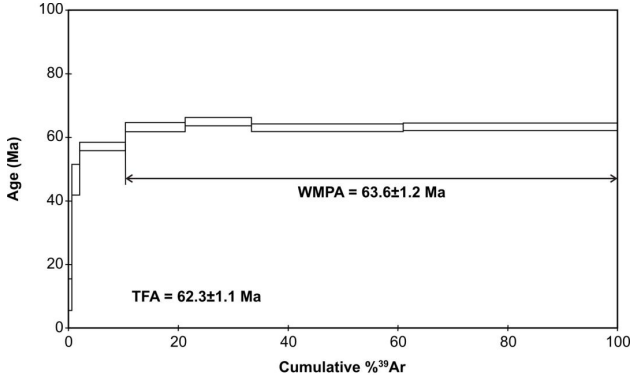

SED
5, 1941–2004, 2013

Table 4c. Whole-rock $^{40}Ar/^{39}Ar$ age data for a lamprophyre dike (Sample No. YK-20) from the island-arc unit in the Ankara Mélange, Turkey.

Sample: YK-20 (whole rock): Lamprophyre, $J = 0.007258 \pm 0.000137$

T °C	^{40}Ar cc (STP)	$^{40}Ar/^{39}Ar$	±1σ	$^{38}Ar/^{39}Ar$	±1σ	$^{37}Ar/^{39}Ar$	±1σ	$^{36}Ar/^{39}Ar$	±1σ	Ca/K	$\sum^{39}Ar$ (%)	Age (Ma) ±1σ	±1σ
550	114.7×10^{-9}	48.724	0.0048	0.014063	0.000040	0.28860	0.00023	0.004714	0.000071	1.04	16.20	45.0	0.9
625	78.3×10^{-9}	71.168	0.0064	0.014657	0.000137	128.516	0.00083	0.006715	0.000045	4.63	23.70	66.0	1.20
700	73.1×10^{-9}	63.482	0.0041	0.014148	0.000062	115.422	0.00187	0.003713	0.000142	4.16	31.70	67.5	1.40
775	85.2×10^{-9}	62.554	0.0032	0.013660	0.000068	0.51460	0.00080	0.003174	0.000096	1.85	41.0	68.3	1.30
850	68.1×10^{-9}	59.659	0.0028	0.013744	0.000112	0.19993	0.00023	0.004958	0.000090	0.72	48.9	58.0	1.10
950	54.6×10^{-9}	58.431	0.0024	0.014092	0.000162	0.29838	0.00075	0.004897	0.000152	1.07	55.3	56.7	1.20
1050	210.7×10^{-9}	50.825	0.0020	0.013886	0.000024	0.61827	0.00022	0.005145	0.000055	2.23	83.8	46.0	0.9
1130	121.2×10^{-9}	51.432	0.0013	0.014028	0.000073	144.061	0.00118	0.005433	0.000056	5.19	100.0	45.7	0.9

Age Spectrum: The sample yielded complex age spectrum with noticeable hump after low temperature step containing three steps intermediate plateau followed by high temperature two steps intermediate Plateau. Intermediate plateaus are characterized accordingly by 24.8 % of ^{39}Ar, Age value of 67.2 ± 1.2 Ma and 44.7 % of ^{39}Ar, Age value of 45.9 ± 0.9 Ma.

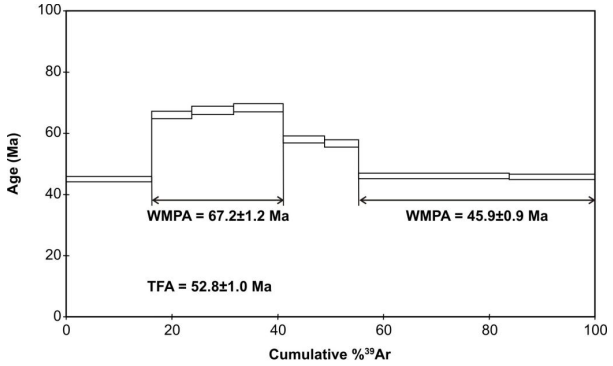

SED
5, 1941–2004, 2013

Table 4d. $^{40}Ar/^{39}Ar$ biotite age data for a syeno-diorite plutonic rock (Sample No. YK-438) from the island-arc unit in the Ankara Mélange, Turkey.

Sample: YK-438 (biotite): Syeno-diorite, $J = 0.004553 \pm 0.000054$

T °C	^{40}Ar cc (STP)	$^{40}Ar/^{39}Ar$	±1σ	$^{38}Ar/^{39}Ar$	±1σ	$^{37}Ar/^{39}Ar$	±1σ	$^{36}Ar/^{39}Ar$	±1σ	Ca/K	$\sum^{39}Ar$ (%)	Age (Ma) ±1σ	±1σ
500	10.2×10^{-9}	61.084	0.0090	0.01989	0.00107	0.7800	0.0026	0.01226	0.00144	2.81	9.0	20.30	3.46
600	14.4×10^{-9}	82.535	0.0136	0.01627	0.00075	15.022	0.0075	0.00992	0.00159	5.41	18.4	43.20	3.79
700	17.3×10^{-9}	121.050	0.0098	0.00960	0.00130	21.617	0.0064	0.01488	0.00069	7.78	26.1	62.22	1.78
800	25.9×10^{-9}	128.671	0.0263	0.01743	0.00152	0.9964	0.0146	0.00617	0.00198	3.59	37.0	88.51	4.68
900	39.8×10^{-9}	126.457	0.0087	0.01645	0.00019	0.8052	0.0025	0.00343	0.00027	2.9	53.9	93.11	1.25
1000	48.8×10^{-9}	126.405	0.0147	0.01668	0.00067	0.4739	0.0055	0.00371	0.00111	1.71	74.8	92.41	2.77
1130	52.0×10^{-9}	111.241	0.0102	0.01900	0.00068	21.389	0.0021	0.00361	0.00065	7.7	100.0	80.77	1.78

Age Spectrum: The sample yielded age spectrum with three steps plateau characterized by 48.6 % of ^{39}Ar, Age value of 92.7 ± 1.2 Ma. On the Inverse Isochrone Plot points don't form linear regression.

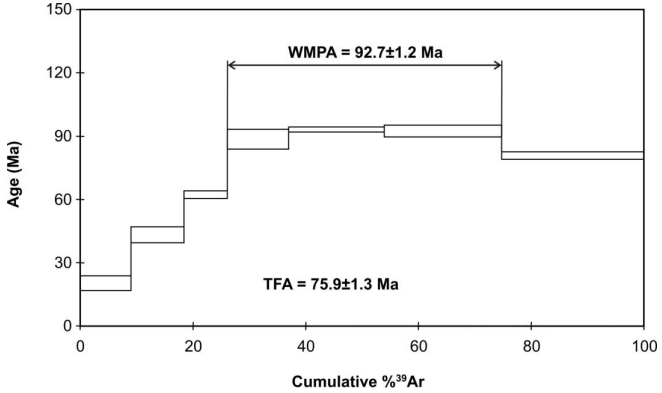

SED
5, 1941–2004, 2013

Table 5. Major, trace element and REE data for a select group of volcanic and dike rocks from the Neotethyan ophiolitic units in the Ankara Mélange (first nine samples from Tankut et al., 1998).

Sample no.	BM1	BM3	BM5	95GK4	95GK6	95GKE4	96GKE51	96GKE57	96GKE58B	CE.07	CE.08
Rock-type	Basalt	Basaltic andesite	Basalt	Dolerite	Dolerite	Dolerite	Dolerite	Dolerite	Dolerite	Basalt	Basalt
Oxide, wt %											
SiO_2	50.53	51.34	50.47	51.08	49.45	51.53	48.93	50.45	47.08	55.50	54.94
TiO_2	1.12	0.26	1.13	1.66	1.68	1.82	0.67	1.74	1.55	0.82	0.81
Al_2O_3	15.96	17.16	15.93	13.45	13.52	12.53	11.00	12.97	11.18	18.43	18.66
Fe_2O_3	10.01	6.80	9.99	11.91	13.23	12.69	9.07	12.31	12.21	8.12	8.47
MnO	0.14	0.12	0.14	0.23	0.22	0.23	0.18	0.23	0.22	0.60	0.63
MgO	6.32	8.17	5.89	7.04	6.41	6.67	10.54	6.30	8.67	3.54	3.81
CaO	4.88	11.07	5.33	9.18	10.91	7.93	15.30	8.66	13.11	1.27	1.17
Na_2O	3.31	2.30	3.34	3.79	2.89	3.89	0.43	3.41	1.22	7.62	7.50
K_2O	0.28	0.28	0.29	0.34	0.36	0.39	0.07	0.37	0.12	0.17	0.19
P_2O_5	0.13	0.07	0.12	0.17	0.21	0.22	0.06	0.21	0.23	0.09	0.10
LOI	6.81	2.05	6.94	1.2	1.04	0.85	3.12	1.69	3.06	3.70	3.50
Total	99.49	99.62	99.57	100.05	99.92	99.75	99.35	98.34	98.65	99.85	99.84
Trace, ppm											
Cr	53.00	166.00	36.00	70.00	84.00	130.00	624.00	134.00	103.00	27.40	20.55
Ni	10.00	101.00	8.00	21.00	25.00	48.00	91.00	59.00	37.00	13.20	11.70
Co										27.90	26.10
Sc				35	38	32	41	35	45		
Rb	11.00	9.00	12.00	4.00	4.00	5.00	2.00	7.00	0.00	2.10	2.40
Ba	242.00		270.00	60.00	503.00	188.00	22.00	185.00	52.00	130.00	110.00
Sr	441.00	100.00	420.00	174.00	510.00	402.00	24.00	208.00	71.00	472.80	494.80
Cs							0.64	24.94	3.91	0.40	0.50
Th	0.47	0.60	0.44	0.00	1.00	3.00	2.00	4.00	3.00	0.60	0.60
U				0.21	0.26	0.29	0.14	0.28	0.28	0.30	0.30
Nb	3.00	2.60	4.00	3.70	5.70	4.00	1.30	3.40	4.80	1.30	1.40
Ta	0.00	0.00	0.00	0.24	0.29	0.25	0.15	0.18	0.29	0.10	0.10
Zr	96.00	21.00	98.00	101.00	126.00	119.00	39.00	91.00	113.00	37.90	43.60
Hf	1.70	0.30	2.20	2.77	3.10	3.14	1.16	2.64	3.13	1.40	1.40
Y	25.00	7.00	25.00	37.00	40.00	41.00	18.00	39.00	39.00	14.50	15.50
V		288		363	383	378	273	462	337	202.00	190.00
Pb					1		1		3	5.9	5.3
REE, ppm											
La	3.90	2.90	4.30	7.42	9.25	9.17	3.03	8.19	9.66	4.00	2.90
Ce	10.70	3.70	8.20	16.67	20.29	19.96	6.18	17.66	21.46	8.30	6.90
Pr				2.31	2.81	2.73	0.83	2.43	2.90	1.31	1.05
Nd	5.70	2.20	6.90	11.64	13.66	13.37	4.44	12.10	14.01	5.90	5.90
Sm	2.90	0.50	3.00	4.07	4.64	4.71	1.67	4.41	4.75	1.71	1.53
Eu	0.90	0.18	1.00	1.43	1.59	1.29	0.70	1.42	1.52	0.49	0.46
Gd				5.14	5.71	5.73	2.31	5.85	6.04	2.08	2.00
Tb	0.60	0.15	0.70	1.02	1.13	1.13	0.46	1.10	1.13	0.41	0.40
Dy				6.78	7.42	7.42	3.12	7.39	7.34	2.54	2.59
Ho				1.47	1.60	1.63	0.70	1.62	1.58	0.57	0.61
Er				4.30	4.59	4.78	2.03	4.58	4.39	1.77	1.84
Tm				0.61	0.65	0.68	0.30	0.67	0.65	0.29	0.31
Yb	3.10	0.96	2.90	3.71	3.94	4.18	1.89	4.09	3.90	1.80	1.90
Lu	0.49	0.16	0.50	0.58	0.63	0.65	0.30	0.63	0.61	0.28	0.32

SED
5, 1941–2004, 2013

Table 6. Major, trace element and REE data for a select group of seamount volcanic rocks from the Ankara Mélange.

Sample no Rock-type	2007KM327 Foidite	DM19 Trachybasalt	KM24 Basanite	KM27 Basanite	KM28 Trachyte	KM121 Tephrrite	KM126 Tephyrite	CM38 Basanite
Oxide, wt %								
SiO_2	39.77	50.15	41.08	44.55	68.47	46.36	44.83	44.26
TiO_2	2.16	2.46	1.64	2.17	0.61	2.10	2.46	2.15
Al_2O_3	15.84	15.90	13.21	15.83	15.16	16.70	15.78	15.75
Fe_2O_3	11.67	9.10	7.75	10.41	3.17	12.04	12.27	10.54
MnO	0.33	0.19	0.12	0.16	0.04	0.18	0.18	0.30
MgO	8.10	3.43	3.91	4.91	0.54	3.12	3.93	9.48
CaO	13.95	5.64	13.78	7.8	1.48	8.59	9.60	4.63
Na_2O	0.57	4.74	5.25	4.15	6.79	4.18	3.78	3.98
K_2O	1.56	1.91	0.45	2.1	1.35	1.81	1.78	0.74
P_2O_5	0.51	0.77	0.464	0.653	0.484	0.89	0.84	0.68
LOI	5.3	5.5	11.8	7.1	1.7	3.8	4.3	7.1
Total	99.81	99.77	99.46	99.84	99.77	99.73	99.72	99.61
Trace, ppm								
Cr	342.45	13.70	232.87	198.62	13.70	13.70	20.55	219.17
Ni	128.00	21	113	106	20	20	20	130.70
Co	40.10	24.3	30.6	36.4	2.2	26.10	32.50	39.30
Sc	25.00	15	18	20	3	5	7	21
Rb	26.80	39.8	7.7	43.5	33.4	18.7	18.1	13.50
Ba	280	135	151	251	379	426	401	371.00
Sr	223.30	368.6	529.6	588.4	294.3	577.9	547.0	740.00
Cs	0.20	1.00	0.1	1.00	0.7	0.10	0.10	0.30
Th	5.90	7.6	4.9	5.8	10.5	8.8	8.0	6.30
U	1.40	1.6	1.5	1.2	1.4	1.9	1.6	1.60
Nb	55.40	74.5	47.2	60.5	96	88.3	82.0	62.40
Ta	3.00	4.5	2.8	3.6	6	5.1	5.2	3.70
Zr	200.40	291.3	187.2	240	389.5	273.4	257.0	252.10
Hf	4.90	6.9	4.6	6.2	10.2	5.7	5.9	6.50
Y	22.70	24.3	20.6	25	34	29.2	29.0	25.60
V	207	136	157	199	14	90	117	168
Pb	4	1.5	5.6	4.9	7.2	5	7.9	1.8
REE, ppm								
La	37.00	54.4	33	43.4	60.7	63.4	61.1	42.30
Ce	73.00	122.0	64.8	83.5	114.7	128.8	122.9	84.90
Pr	8.80	13.61	7.8	9.71	14.25	13.73	13.57	9.87
Nd	34.30	54.0	29.1	37.3	49	50.7	51.0	39.90
Sm	6.11	9.76	5.21	6.56	8.05	9.06	9.04	6.64
Eu	2.03	3.17	1.74	2.11	2.19	2.84	2.99	2.16
Gd	5.78	8.46	4.65	5.81	6.67	8.33	8.33	6.21
Tb	0.88	1.17	0.76	0.93	1.15	1.18	1.21	0.93
Dy	4.49	5.56	4.01	4.89	6.34	5.88	5.90	4.72
Ho	0.82	0.87	0.76	0.93	1.21	1.07	1.06	0.91
Er	2.11	1.94	2	2.48	3.42	2.72	2.63	2.68
Tm	0.33	0.25	0.29	0.36	0.51	0.36	0.36	0.38
Yb	1.85	1.36	1.71	2.07	3.27	2.18	2.17	2.10
Lu	0.28	0.17	0.25	0.31	0.47	0.30	0.30	0.33

SED
5, 1941–2004, 2013

Table 7. Major, trace element and REE data for a select group of island-arc volcanic and syenodiorite rocks from the Ankara Mélange.

Sample no Rock-type	04.NAM Syeno-diyorite	05.NAM Syeno-diyorite	06.NAM Syeno-diyorite	DM35 Tephrite	DM 36 Tephrite	DM37 Foidite	CE960 Basanite	08CM01 Leucite Tephrite	08CM07 Basanite	KM54 Basanite
Oxide, wt %										
SiO_2	50.31	49.35	49.11	41.65	41.86	39.81	42.41	48.29	45.00	46.34
TiO_2	0.59	0.61	0.62	0.76	0.74	0.70	0.89	0.67	0.79	0.93
Al_2O_3	18.69	18.75	18.39	15.90	15.55	12.84	16.89	18.21	14.57	14.36
Fe_2O_3	8.45	8.77	8.42	10.82	9.31	8.90	12.38	9.15	11.21	11.03
MnO	0.17	0.19	0.19	0.15	0.15	0.14	0.25	0.25	0.21	0.18
MgO	2.25	2.45	2.39	7.23	7.35	10.81	7.5	4.23	6.28	6.33
CaO	6.38	7.14	6.82	3.51	4.08	5.36	11.17	7.91	12.22	9.64
Na_2O	2.68	2.57	2.35	0.57	0.46	0.21	2.48	3.78	2.56	2.79
K_2O	5.32	5.07	5.68	5.99	6.15	5.15	0.62	2.91	2.15	3.09
P_2O_5	0.48	0.49	0.49	0.44	0.41	0.24	0.42	0.46	0.33	0.44
LOI	4.30	4.20	5.10	12.7	13.6	15.4	4.7	3.7	4.2	4.5
Total	99.61	99.58	99.63	99.69	99.68	99.61	99.71	99.56	99.52	99.67
Trace, ppm										
Cr	47.94	82.19	47.94	13.70	20.55	342.45	21	14.00	130.00	61.64
Ni	20	20	20	23	41	156	43	5.00	24.50	39.00
Co	20.60	22.80	20.70	25.7	28.0	38.4	43.1	24.80	37.10	36.20
Sc	11	11	11	20	21	37	30	20.00	48.00	39.00
Rb	140.2	138.5	148.2	184.1	172.6	162.6	18.3	52.50	29.40	195.80
Ba	1685	1557	1520	783	739	887	577	1883	1051	840
Sr	845.2	915.3	759.4	257.5	331.3	362.2	563.5	742.60	779.80	934.80
Cs	1.1	2.1	3.5	6	4.5	3.4	0.9	3.10	1.20	1.50
Th	11.9	13.9	11.1	10.1	10.3	7.5	4.7	18.00	5.90	5.30
U	3.2	3.1	3.0	3.3	3.7	1.8	1.5	2.40	1.70	2.20
Nb	8.9	9.4	7.6	9.1	8.7	4.2	4	12.30	5.10	3.40
Ta	0.4	0.4	0.3	0.3	0.4	0.1	0.3	0.50	0.20	0.20
Zr	76.1	86.0	72.9	72.8	74.4	49.2	68.9	87.80	57.70	75.20
Hf	1.6	2.2	2.0	2.0	1.7	1.4	2	2.50	1.60	2.00
Y	23.6	23.0	20.3	14.8	16.5	12.5	21.4	20.90	18.70	22.00
V	169	182	166	279	275	260	339	273	301	302
Pb	4	21.8	24.9	3.9	7.4	6.1	5.2	7.3	5.5	9
REE, ppm										
La	33.7	36.6	31.9	26.0	25.7	18.8	20	36.70	20.70	18.40
Ce	60.0	63.7	55.4	53.2	53.5	37.7	42.6	66.70	40.00	41.90
Pr	6.72	7.12	6.20	5.85	5.63	3.93	5.52	7.87	4.89	5.51
Nd	25.3	25.7	24.9	23.0	22.5	15.7	25	32.80	20.70	22.90
Sm	4.91	4.88	4.41	4.42	4.29	3.21	5.27	5.81	4.18	5.12
Eu	1.32	1.31	1.24	1.18	1.21	0.91	1.57	1.53	1.33	1.47
Gd	4.70	4.51	4.18	3.89	4.02	3.21	5.12	5.23	4.31	5.17
Tb	0.70	0.71	0.64	0.57	0.60	0.47	0.79	0.76	0.66	0.80
Dy	3.89	4.11	3.73	2.83	3.28	2.52	4.03	3.88	3.54	4.34
Ho	0.72	0.75	0.67	0.56	0.60	0.46	0.76	0.73	0.69	0.81
Er	2.02	2.14	1.92	1.60	1.61	1.24	2.07	2.05	2.00	2.14
Tm	0.30	0.30	0.28	0.21	0.23	0.17	0.32	0.28	0.29	0.34
Yb	2.16	2.05	1.89	1.49	1.47	1.10	1.82	1.84	1.65	1.94
Lu	0.28	0.33	0.25	0.22	0.23	0.16	0.28	0.27	0.26	0.30
Mg#	35	36	36	57	61	71	55	48	53	53
KO/NaO	1.99	1.97	2.42	10.51	13.37	24.52	0.25	0.77	0.84	1.11

SED
5, 1941–2004, 2013

Table 8. Major, trace element and REE data for a select group of island-arc volcanic rocks from the Ankara Mélange.

Sample no Rock-type	CE.962 Basanite	CE.964 Basanite	CS.07 Basanite	CS.11 Basanite	CE.96 Basalt	CE.98 Basalt	CS.99 Basalt	MS.34 Basanite	MS.35 Basanite	MS.36 Basaltic-trachyandesite	COR.6 Basanite	COR.7 Trachy basalt	COR.9 Trachy basalt	COR.10 Basanite
Oxide, wt %														
SiO_2	42.28	42.78	44.35	42.69	51.27	48.78	48.28	44.49	44.56	54.26	44.13	48.08	46.26	42.86
TiO_2	0.88	0.9	0.78	0.82	0.78	1.74	1.71	1.00	0.92	0.50	0.84	0.84	0.85	0.93
Al_2O_3	16.57	16.84	16.10	16.55	15.91	14.85	14.89	17.60	15.63	17.93	17.26	17.21	18.47	17.03
Fe_2O_3	12.07	12.26	11.44	11.98	9.57	12.69	12.69	9.35	10.31	6.34	9.40	10.17	9.49	10.21
MnO	0.27	0.24	0.21	0.20	0.14	0.20	0.20	0.16	0.19	0.14	0.18	0.19	0.16	0.20
MgO	8	7.37	7.67	6.68	6.44	5.78	5.72	6.82	8.84	2.44	7.21	4.22	4.13	4.74
CaO	10.83	10.42	10.47	9.48	7.64	8.26	8.54	9.17	9.84	5.97	8.84	6.9	8.19	13.37
Na_2O	2.7	2.47	3.29	3.88	4.73	3.84	3.48	2.09	2.15	3.75	2.89	4.32	2.35	1.28
K_2O	0.73	1.57	0.51	1.06	0.12	0.59	0.75	2.39	2.33	4.10	2.82	2.51	3.01	2.41
P_2O_5	0.38	0.43	0.33	0.39	0.06	0.18	0.16	0.31	0.31	0.27	0.39	0.46	0.34	0.44
LOI	5	4.3	4.5	6.0	3.1	2.7	3.1	6.2	4.5	4	5.6	4.6	6.4	6.1
Total	99.71	99.58	99.65	99.69	99.81	99.57	99.47	99.64	99.61	99.67	99.56	99.48	99.67	99.62
Mg#	57	54	57	52	57	47	47	59	63	43	60	45	46	48
Trace, ppm														
Cr	21	14	68	14	14	41	41	21	82	14	55	14	27	41
Ni	29	37	31.00	19.70	20.40	18.60	18.00	12.20	23.00	5.10	16.7	1.9	15.1	17.5
Co	44.5	43.7	44.10	43.40	31.80	40.10	40.70	33.20	40.60	14.70	32.4	26.5	24.1	40.2
Sc	32	31	41	34	35	37	37	34	49	11	31	15	26	33
Rb	46.5	65.1	11.00	42.50	3.20	8.30	10.00	58.50	55.70	129.20	67.7	38.3	92.4	59.3
Ba	636	2044	596.00	613.00	36.00	882.00	1437.00	796.00	700.00	1225.00	885	2166	902	877
Sr	497.4	620.5	471.90	321.40	43.40	1129.10	1385.20	497.00	460.50	546.70	966.6	875.8	579.5	660.2
Cs	1.3	1	2.90	1.50	32.70	0.70	0.40	2.90	2.70	3.70	4.4	2.1	2.8	2.5
Th	3.8	4.3	3.70	3.90	0.30	0.90	0.90	12.70	11.00	22.90	14.3	12.1	14.3	15.8
U	1	1.2	1.50	1.10	0.10	0.20	0.30	3.20	2.90	5.70	3.6	3	3.1	4.1
Nb	3.1	3.8	4.90	5.40	4.70	7.40	7.10	7.40	6.30	10.30	5.9	6.3	6.4	5.9
Ta	0.2	0.3	2.40	1.60	3.30	3.50	3.90	0.90	1.00	1.50	0.3	0.3	0.4	0.3
Zr	63.3	65	50.60	55.20	46.10	107.30	104.80	110.90	106.30	175.80	126.4	94.4	108.3	113.3
Hf	2.2	1.9	1.50	1.60	1.50	2.90	2.90	2.90	2.90	4.10	3.1	2.6	2.6	2.3
Y	19.6	20.7	18.20	19.80	20.30	34.00	34.10	25.80	24.80	27.10	25.3	24.3	20.4	23.8
V	357	357	365	339	335	379	385	364.00	401.00	157.00	292	282	280	388
Pb	3.6	4.8	5.40	8.30	0.7	0.4	0.6	8.9	8.9	7	13.4	17.5	13.1	18.8

SED
5, 1941–2004, 2013

Table 8. Continued.

Sample no Rock-type	CE.962 Basanite	CE.964 Basanite	CS.07 Basanite	CS.11 Basanite	CE.96 Basalt	CE.98 Basalt	CS.99 Basalt	MS.34 Basanite	MS.35 Basanite	MS.36 Basaltic-trachyandesite	COR.6 Basanite	COR.7 Trachy basalt	COR.9 Trachy basalt	COR.10 Basanite
REE, ppm														
La	17.3	17.6	14.90	16.80	3.00	8.40	8.30	37.60	33.30	60.20	43.1	36.2	41.1	43.8
Ce	37.6	39.5	31.60	35.20	7.70	20.90	20.40	73.30	67.00	109.70	90.9	74.4	82.0	92.2
Pr	5.16	5.27	4.16	4.63	1.10	2.90	2.84	8.63	8.13	11.97	9.92	8.46	8.73	9.80
Nd	22.7	23	17.60	20.10	5.20	14.50	13.70	34.50	32.80	43.60	35.3	34.6	31.1	34.8
Sm	4.99	5.22	4.14	4.70	1.86	3.92	3.95	6.88	6.66	7.35	7.23	6.81	5.85	6.93
Eu	1.51	1.53	1.27	1.38	0.74	1.26	1.43	1.94	1.80	1.87	1.96	1.86	1.55	1.79
Gd	4.87	4.94	3.97	4.36	2.49	5.00	5.13	6.21	5.88	5.83	6.42	6	5.30	6.23
Tb	0.72	0.73	0.63	0.70	0.52	0.96	0.97	0.95	0.92	0.90	0.94	0.92	0.76	0.89
Dy	3.92	4.06	3.23	3.47	3.17	5.54	5.76	4.85	4.66	4.68	4.80	4.83	3.66	4.48
Ho	0.71	0.75	0.63	0.68	0.70	1.23	1.23	0.96	0.86	0.91	0.89	0.88	0.76	0.84
Er	1.88	1.96	1.75	1.79	2.17	3.59	3.50	2.46	2.35	2.58	2.44	2.62	2.06	2.28
Tm	0.3	0.31	0.25	0.29	0.33	0.55	0.56	0.39	0.36	0.42	0.35	0.36	0.30	0.34
Yb	1.78	1.78	1.56	1.67	2.11	3.35	3.34	2.38	2.23	2.67	2.27	2.33	1.86	2.19
Lu	0.27	0.27	0.24	0.25	0.33	0.52	0.51	0.36	0.33	0.42	0.35	0.36	0.29	0.33
K_2O/Na_2O	0.27	0.64	0.16	0.27	0.03	0.15	0.22	1.14	1.08	1.09	0.98	0.58	1.28	1.88

SED
5, 1941–2004, 2013

Table 9. Major, trace element and REE data for a select group of lamprophyric dike rocks from the Ankara Mélange.

Sample no Rock-type	DM2 Tephrite	DM3 Tephrite	DM4 Tephrite	DM5 Tephrite	DM5A Tephrite	DM6 Trachy-basalt	DM7 Phono tephrite	DM7A Tephrite	DM8 Trachy-basalt	DM9 Phono tephrite	DM10 Phono tephrite	DM17 Tephrite	CE1206 Picro-basalt	CE1207 Picro-basalt	CE2 Picro-basalt	CE1210 Trachy-basalt	25BM11 Trachy andesite
Oxide, wt %																	
SiO_2	45.25	43.02	47.41	45.84	46.23	48.59	50.29	50.49	49.34	47.48	47.02	46.45	41.94	47.34	44.89	51.33	58.15
TiO_2	0.69	0.76	0.58	0.64	0.66	0.73	0.62	0.62	0.70	0.73	0.74	0.78	1.12	0.83	1.26	1.24	0.43
Al_2O_3	11.20	10.93	15.79	16.98	17.00	10.34	14.94	14.73	12.10	14.37	14.66	11.40	12.91	15.66	13.36	15.62	17.43
Fe_2O_3	11.16	12.10	9.54	10.86	11.03	11.46	10.85	10.72	10.92	11.07	11.13	12.59	10.8	9.79	11.12	7.33	5.81
MnO	0.23	0.22	0.23	0.21	0.21	0.22	0.20	0.18	0.21	0.24	0.23	0.22	0.2	0.21	0.22	0.08	0.14
MgO	5.41	4.98	2.90	4.66	4.87	6.02	4.02	4.13	4.49	3.43	3.50	5.09	7.71	4.02	8.23	5.99	**1.88**
CaO	14.50	15.89	12.25	10.25	9.57	13.68	7.30	7.53	13.50	8.44	8.53	12.26	16.47	9.11	14.37	8.22	4.04
Na_2O	0.67	0.28	0.36	1.63	1.68	0.56	2.84	2.78	1.96	2.64	2.95	1.58	1.62	2.97	1.70	3.95	5.56
K_2O	5.47	5.54	6.96	4.67	4.99	5.73	5.53	5.50	4.11	6.34	5.82	5.40	**0.72**	4.5	1.01	1.85	4.32
P_2O_5	0.89	0.80	0.45	0.44	0.40	1.08	0.96	0.93	0.89	0.78	0.78	0.90	0.49	0.64	0.55	0.75	0.29
LOI	4	4.9	2.9	3.4	3.0	1.1	2.0	1.9	1.3	3.7	3.9	2.8	5.8	4.6	2.9	3.4	1.6
Total	99.5	99.46	99.42	99.61	99.60	99.49	99.53	99.53	99.52	99.27	99.28	99.48	99.78	99.67	99.64	99.76	99.64
Trace, ppm																	
Cr	13.70	13.70	13.70	13.70	13.70	13.70	13.70	13.70	13.70	13.70	13.70	13.70	89	21	82	**158**	68
Ni	20	20	20	20	20	20	20	20	20	20	20	20	48	28	67	86	45
Co	33.0	39.4	26.9	34.8	34.5	37.9	34.1	33.8	32.2	28.5	28.9	41.2	35.5	24.2	39.7	24.9	12.50
Sc	30	34	10	25	27	45	24	25	30	21	22	36	41	22	39	19	7
Rb	51.4	52.6	94.6	76.9	81.5	46.9	65.0	67.7	29.7	47.3	43.1	50.0	20.8	75.5	13.8	29.9	76.5
Ba	1861	1881	2899	1224	1228	1760	1183	1233	1846	3229	3172	2019	180	1109	257	475	1456
Sr	697.0	864.1	762.5	701.6	811.3	823.9	1483.3	1401.6	758.9	1287.1	1335.2	790.0	1073	1116	805.4	1006	679.1
Cs	0.1	0.1	0.2	0.3	0.2	0.1	0.1	0.1	0.1	0.4	0.4	0.1	0.3	0.6	0.1	0.2	0.1
Th	24.4	14.0	19.7	8.9	9.1	21.9	14.2	14.4	23.1	34.6	33.6	13.2	7.3	14.9	6.9	5.4	25.0
U	6.0	5.6	7.4	2.9	3.1	5.4	7.1	6.9	6.0	10.1	10.5	5.1	2.4	4.9	2.5	1.0	6.9
Nb	18.3	22.7	18.4	7.8	7.9	17.0	13.7	13.9	18.6	34.1	33.9	21.7	9.7	13.1	15.1	7.4	10.7
Ta	0.6	0.7	0.7	0.3	0.3	0.7	0.5	0.5	0.6	1.1	1.2	0.7	0.6	0.9	1.0	1	0.6
Zr	111.4	111.2	117.3	65.0	62.3	103.2	95.1	93.8	112.6	188.1	186.3	101.6	92.9	163.5	111.9	121.9	199.7
Hf	2.8	2.9	2.8	1.6	1.4	2.7	2.5	2.3	2.8	4.7	4.4	2.6	2.5	4.1	2.8	3.1	4.3
Y	23.7	24.5	22.1	16.2	15.1	24.4	21.5	20.4	24.8	34.2	34.4	23.7	21.9	34.8	24.7	16.9	28.9
V	305	403	405	307	299	329	262	269	347	329	329	370	300	245	330	162	116
Pb	32.3	17.0	11.1	16.8	15.5	14.8	9.6	8.8	9.4	12.6	11.3	20.2	2.3	6.6	0.9	1.30	33.9
Mg#	49	45	38	46	47	51	42	43	45	38	38	44	59	45	59	62	39
KO/NaO	8.16	19.79	19.33	2.87	2.97	10.23	1.95	1.98	2.10	2.40	1.97	3.42	0.44	1.52	0.59	0.47	0.78

SED
5, 1941–2004, 2013

Table 9. Continued.

Sample no Rock-type	DM2 Tephrite	DM3 Tephrite	DM4 Tephrite	DM5 Tephrite	DM5A Tephrite	DM6 Trachy-basalt	DM7 Phono tephrite	DM7A Tephrite	DM8 Trachy-basalt	DM9 Phono tephrite	DM10 Phono tephrite	DM17 Tephrite	CE1206 Picro-basalt	CE1207 Picro-basalt	CE2 Picro-basalt	CE1210 Trachy-basalt	25BM11 Trachy andesite
REE, ppm																	
La	60.0	41.8	49.5	26.4	25.0	56.6	32.2	30.7	58.4	83.6	81.2	41.4	26.3	43.2	29.3	33.3	69.2
Ce	120.4	87.4	97.8	52.4	49.7	115.9	69.8	67.3	119.6	159.0	156.7	86.5	53.1	88.9	58.1	70.7	124.9
Pr	13.07	9.79	10.41	5.75	5.52	13.12	7.99	7.71	13.19	16.87	16.92	9.76	6.83	10.9	7.52	8.76	13.24
Nd	49.9	39.3	38.7	22.2	22.3	53.9	32.7	32.0	51.5	63.2	63.9	39.6	28.2	42.5	29.8	33.1	46.9
Sm	9.36	8.07	7.17	4.49	4.29	9.83	6.15	5.93	9.48	11.52	11.64	7.84	5.98	8.52	6.96	5.67	7.82
Eu	2.26	2.02	1.86	1.20	1.14	2.35	1.53	1.50	2.27	2.84	2.88	2.00	1.72	2.49	1.98	1.59	1.93
Gd	7.94	7.09	6.23	4.01	3.88	8.37	5.32	5.22	7.97	10.04	10.03	7.19	5.68	8.09	6.36	4.56	6.22
Tb	1.04	0.97	0.88	0.59	0.56	1.07	0.77	0.76	1.07	1.36	1.36	0.95	0.86	1.21	0.93	0.67	0.90
Dy	4.95	4.71	4.31	2.95	2.97	4.94	3.94	3.91	4.88	6.88	6.66	4.72	4.06	6.33	4.68	3.28	4.98
Ho	0.82	0.82	0.73	0.55	0.55	0.79	0.74	0.73	0.84	1.16	1.19	0.80	0.79	1.2	0.81	0.61	0.91
Er	2.05	2.12	2.00	1.50	1.45	2.10	1.96	1.94	2.08	3.08	3.02	2.10	2.09	3.27	2.30	1.64	2.63
Tm	0.29	0.29	0.27	0.22	0.21	0.28	0.29	0.27	0.29	0.43	0.44	0.30	0.32	0.52	0.33	0.25	0.42
Yb	1.65	1.79	1.83	1.41	1.33	1.69	1.74	1.76	1.69	2.67	2.80	1.73	1.76	2.94	1.89	1.47	2.66
Lu	0.25	0.27	0.26	0.21	0.20	0.25	0.27	0.26	0.25	0.41	0.41	0.26	0.27	0.46	0.27	0.22	0.43
$^{87}Sr/^{86}Sr$		0.704786			0.704892			0.704697	0.704720			0.704797			0.704820		
$^{143}Nd/^{144}Nd$		0.512681			0.512686			0.512690	0.512682			0.512680			0.512674		
$^{206}Pb/^{204}Pb$		19.540			19.332			19.939	19.604			19.594			19.418		
$^{207}Pb/^{204}Pb$		15.662			15.655			15.691	15.675			15.659			15.664		
$^{208}Pb/^{204}Pb$		39.376			39.192			39.612	39.536			39.407			39.297		

SED
5, 1941–2004, 2013

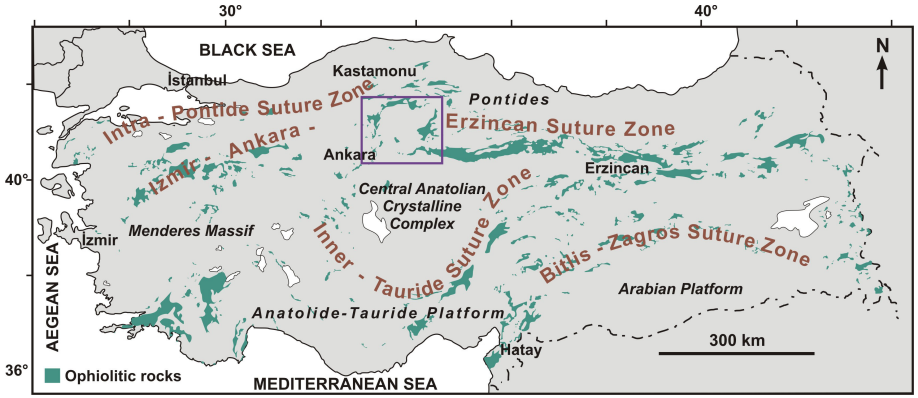

Fig. 1. Simplified ophiolite map of Turkey showing the distribution of the suture zones and some of the major tectonic entities in Turkey (from MTA, 2001). The inset box refers to the map area in Fig. 2.

SED
5, 1941–2004, 2013

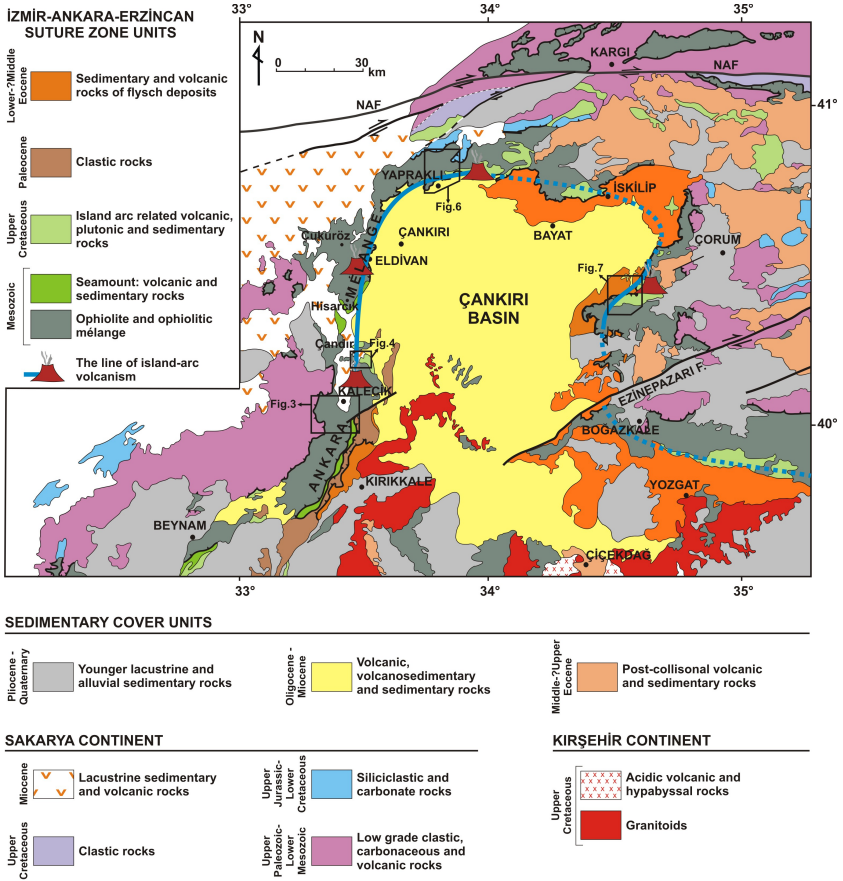

Fig. 2. Geological map of the Çankırı–Çorum area along the IAESZ in north-central Turkey (modified after Uğuz et al., 2002).

SED
5, 1941–2004, 2013

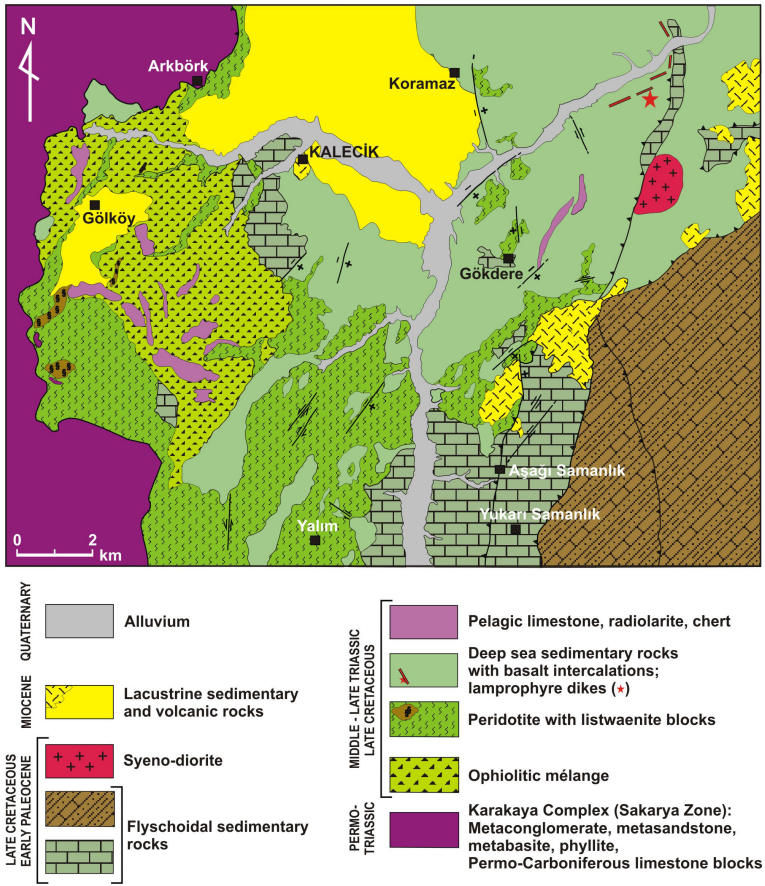

Fig. 3. Geological map of the Kalecik area, east of Ankara, showing the distribution of the ophiolitic, turbiditic and island-arc rock units in the Ankara Mélange in north-central Turkey.

SED
5, 1941–2004, 2013

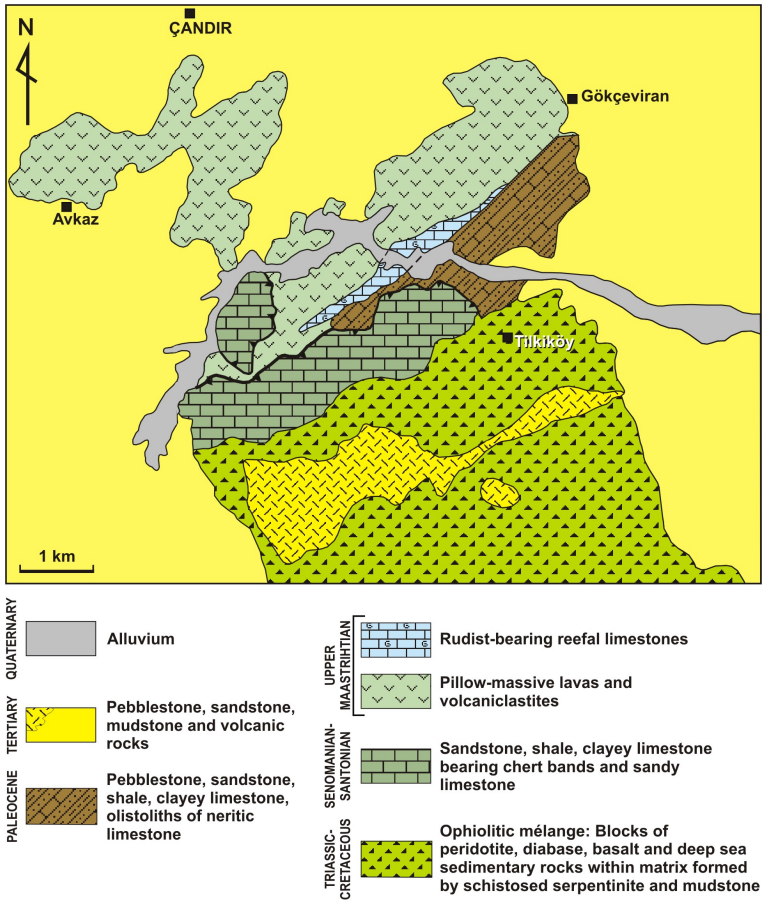

Fig. 4. Geological map of the northern part of the Kalecik area (modified after Hakyemez et al., 1986).

SED
5, 1941–2004, 2013

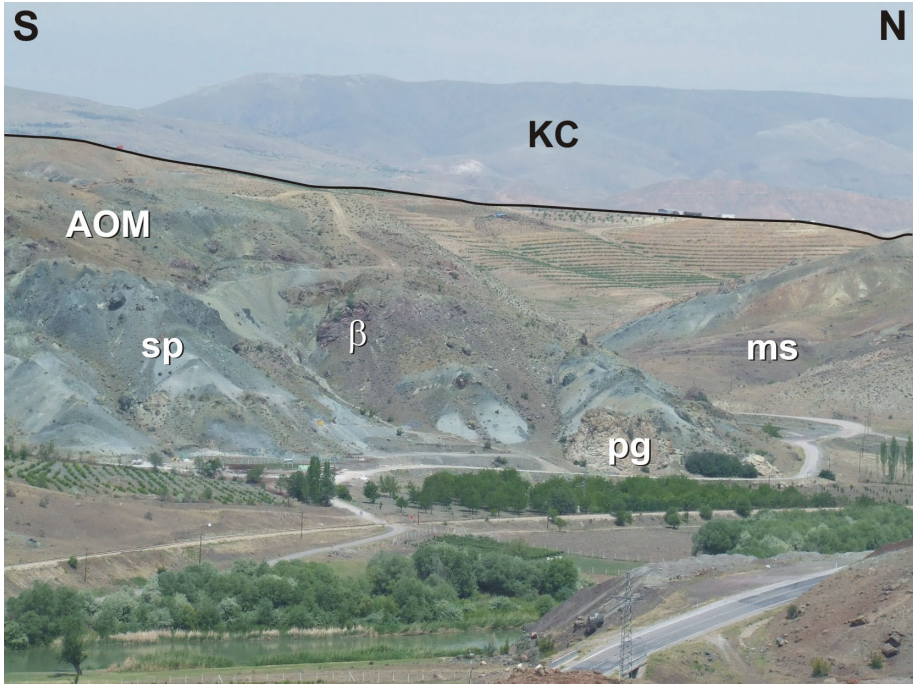

Fig. 5. View of the Ankara Mélange and the Karakaya Complex (Sakarya Continent). Key to lettering: AOM = Ankara Mélange, β = basalt, KC = Karakaya Complex, ms = mudstone, pg = plagiogranite, sp = serpentinized peridotites.

SED
5, 1941–2004, 2013

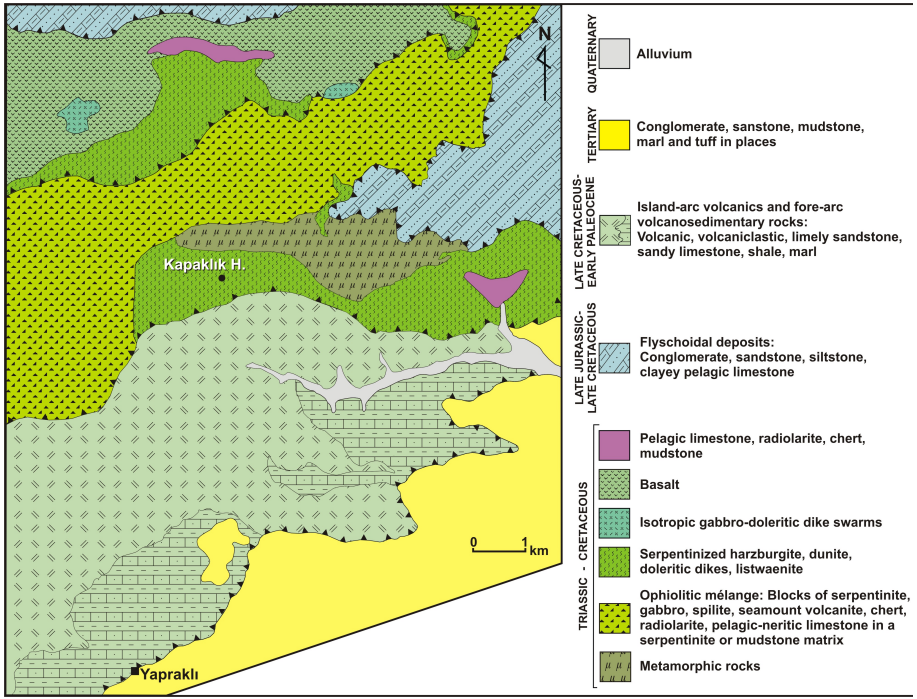

Fig. 6. Simplified geological map of the Yapraklı–Çankırı area, showing the distribution of the ~180 Ma Neotethyan ophiolitic units, ophiolitic mélange and island-arc rocks.

SED
5, 1941–2004, 2013

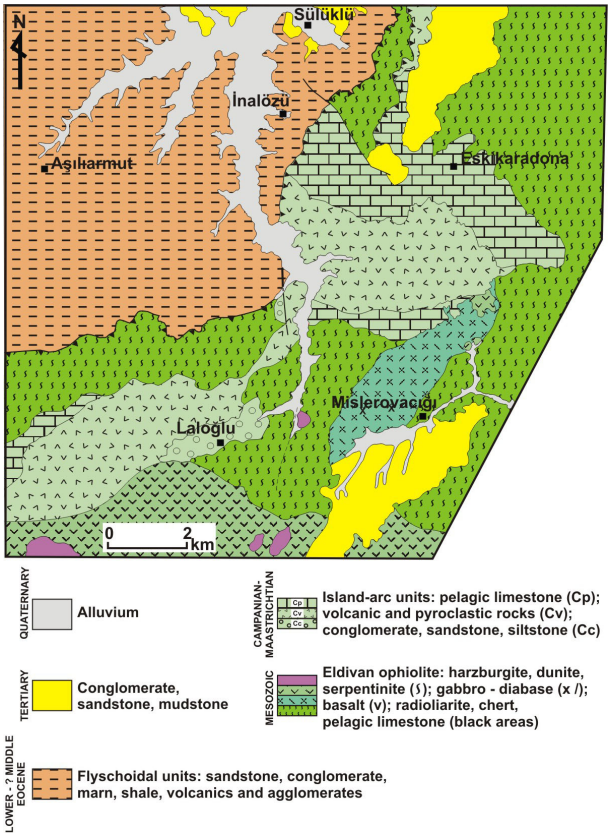

Fig. 7. Geological map of the Laloglu (Çorum) area, showing the Neotethyan Eldivan ophiolite and the island-arc rock units.

SED
5, 1941–2004, 2013

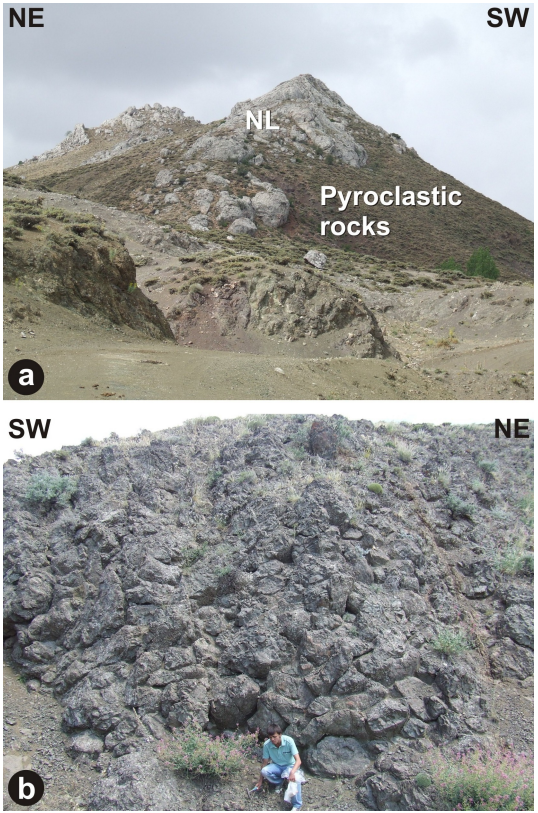

Fig. 8. (a) Neritic limestone covering the seamount volcanic-volcaniclastic rocks in the Ankara Mélange. **(b)** Seamount pillow lavas in the Ankara Mélange. NL = neritic limestone.

SED
5, 1941–2004, 2013

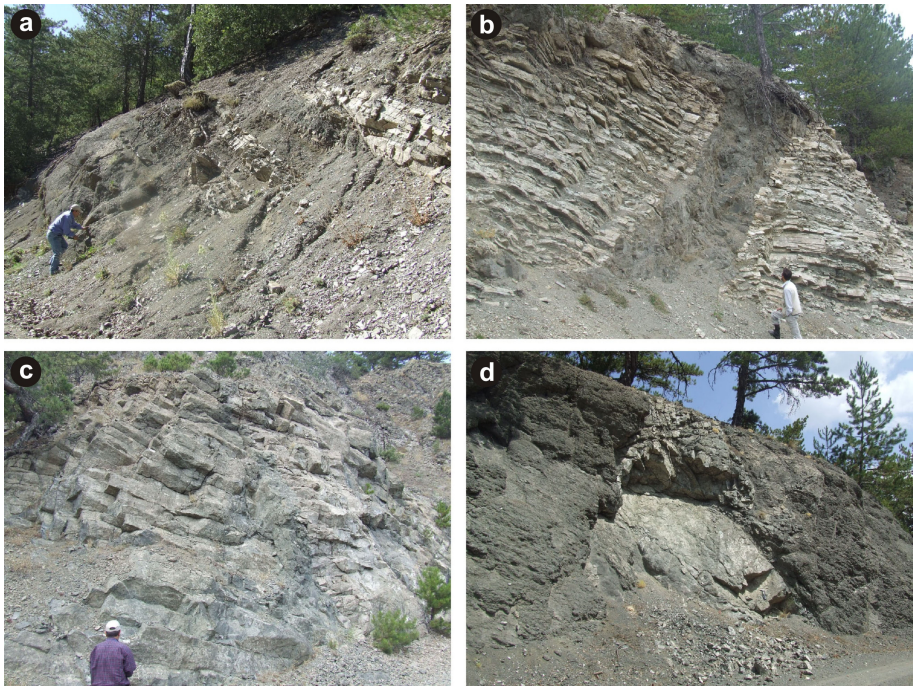

Fig. 9. (a) Limestone-volcanic sandstone intercalation in the island-arc sequence. **(b)** A mafic dike (island-arc origin) crosscutting the pelagic limestone rocks. **(c)** Alkaline basaltic rocks with columnar joint structures. **(d)** Arc volcaniclastic rocks intruded by basaltic to andesitic dikes.

SED
5, 1941–2004, 2013

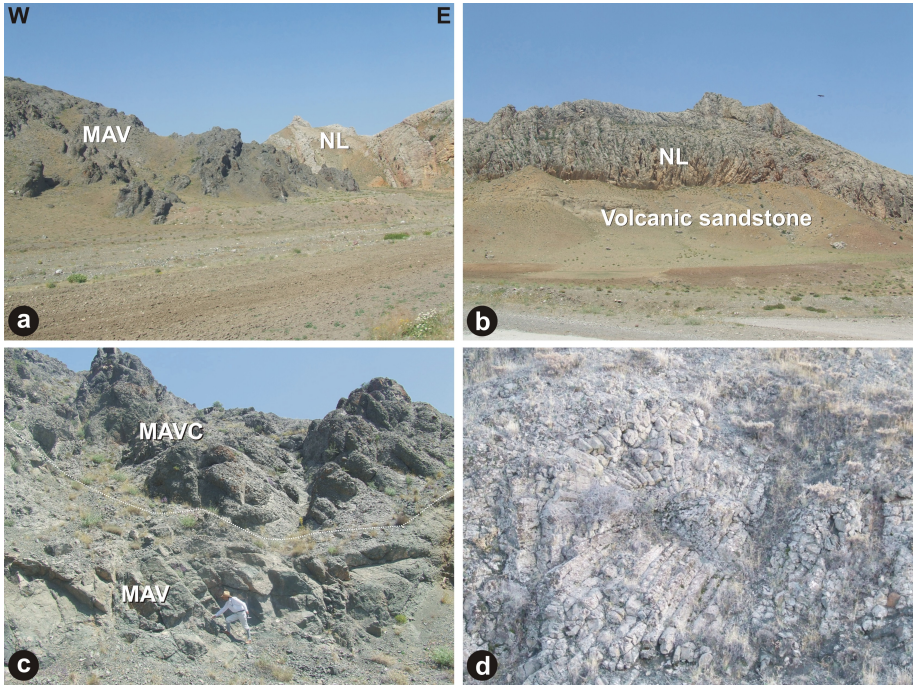

Fig. 10. (a) Upper Cretaceous reefal limestone with rudist fossils unconformably overlying the arc volcanic rocks. **(b)** Reefal limestone underlain by volcanic sandstone. **(c)** Alkaline pillow lavas overlain by volcanic sandstone-pebblestone. **(d)** Alkaline pillow lavas with radial joint structures. All rocks in **(a)** through **(d)** represent the island-arc units.

SED
5, 1941–2004, 2013

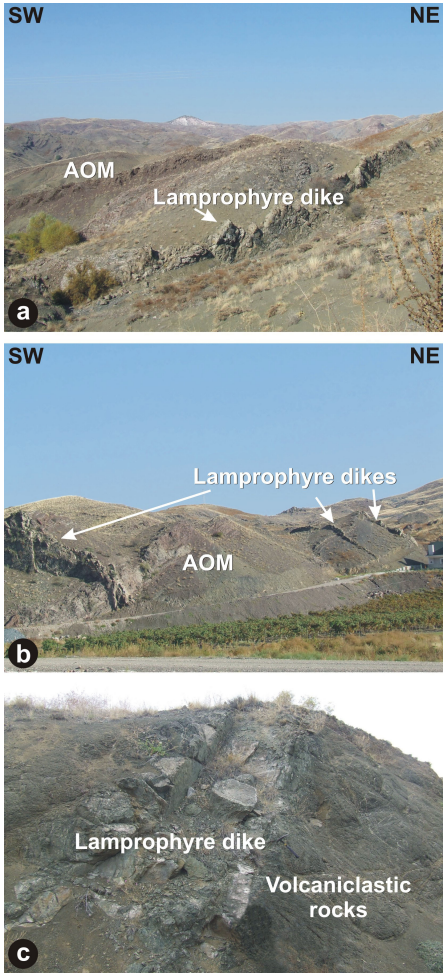

Fig. 11. Lamprophyric dikes crosscutting various lithological units in the Ankara Mélange.

SED
5, 1941–2004, 2013

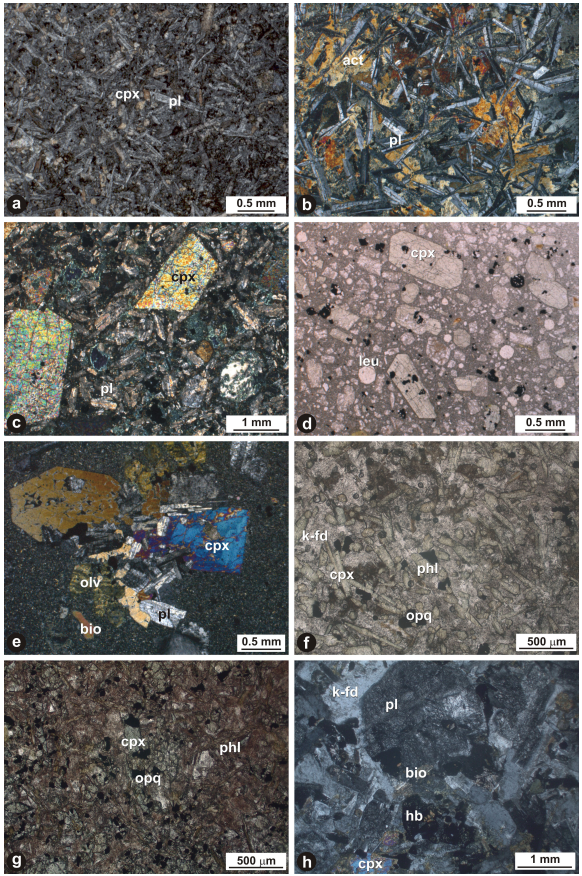

Fig. 12. Photomicrographs of **(a)** a seamount alkaline basalt sample. **(b)** Doleritic dike rock of the 180 Ma Neotethyan oceanic crust. **(c)** Island-arc alkaline basalt sample in cross-polarized light. **(d)** Island-arc alkaline basalt sample in plane-polarized light. **(e)** Island-arc basaltic andesite dike, showing a glomeroporphyritic texture. **(f)** Lamprophyric dike rock with small prismatic cpx (diopside) in a feldspar + phlogopite groundmass (plane-polarized light). **(g)** Lamprophyric dike rock with small prismatic cpx (diopside and phlogopite). **(h)** Syeno-dioritic pluton rock with plagioclase (altered to clay minerals) and biotite + hornblende and minor cpx (cross-polarized light).

SED
5, 1941–2004, 2013

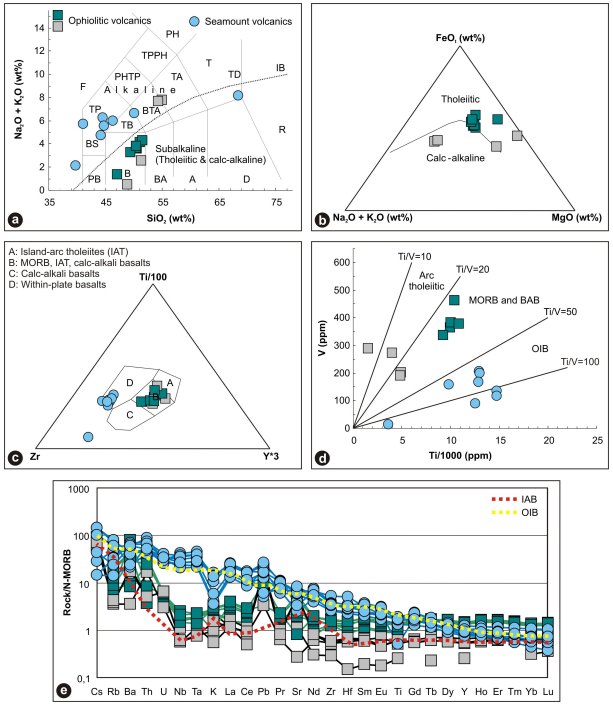

Fig. 13. Geochemical classification of ophiolitic and seamount volcanic rocks. **(a)** Total alkali vs. SiO_2 diagram (Le Bas et al., 1986). **(b)** AFM diagram (Irvine and Baragar, 1971). **(c)** Ti–Zr–Y discrimination diagram (Pearce and Cann, 1973). **(d)** Ti–V diagram (Shervais, 1982). **(e)** N-MORB-normalized multi-element diagrams of the most representative samples (normalization values from Sun and McDonough, 1989). Key to lettering: A = andesite, B = basalt, BA = basaltic andesite, BS = basanite, BTA = basaltic trachyandesite, D = dacite, F = foidite, PC = picrobasalt, PH = phonolite, PHTP = phonotephrite, R = rhyolite, T = trachyte, TA = trachyandesite, TB = trachybasalt, TD = trachydacite, TP = tephrite. IB = alkali-subalkali subdivision from Irvine and Baragar (1971).

SED
5, 1941–2004, 2013

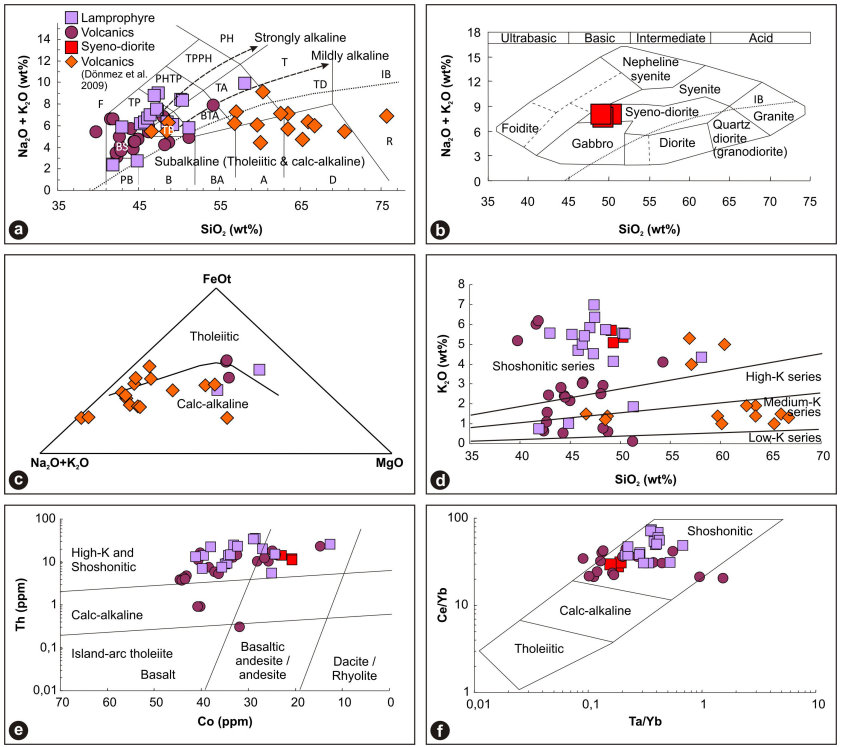

Fig. 14. Geochemical classification of island-arc rocks. **(a)** Total alkali vs. SiO_2 diagram (Le Bas et al., 1986). **(b)** TAS diagram (Cox et al., 1979) for syeno-dioritic pluton rocks. **(c)** Alk–MgO–FeO_t diagram (Irvine and Baragar, 1971) of the subalkaline arc volcanic units (Dönmez et al., 2009, and this study). **(d)** K_2O vs. SiO_2 diagram (Peccerillo and Taylor, 1976). **(e)** Th vs. Co diagram (Hastie et al., 2007). Ce/Yb vs. Ta/Yb diagram (Pearce, 1982).

SED
5, 1941–2004, 2013

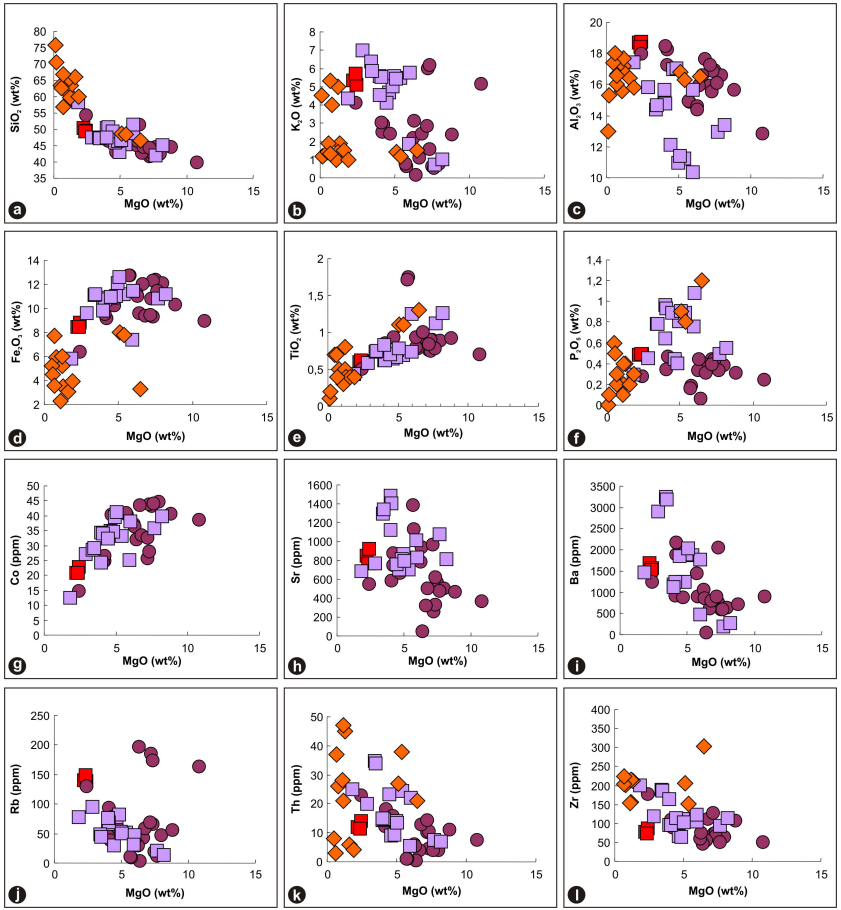

Fig. 15. Major oxides and trace elements vs. MgO variation diagrams for various alkaline island-arc units.

SED
5, 1941–2004, 2013

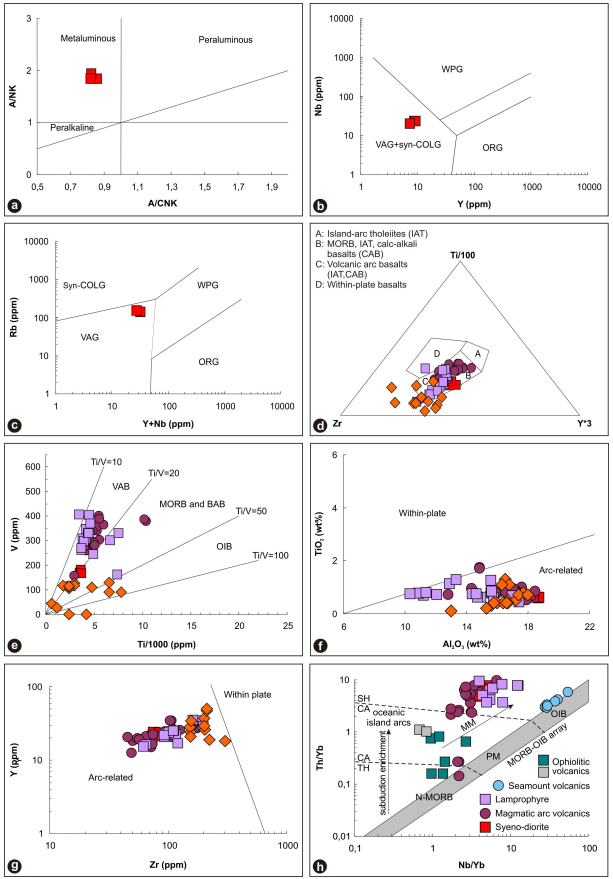

Fig. 16. **(a)** A/CNK, molar $Al_2O_3/(CaO + Na_2O + K_2O)$ vs. A/NK, molar $Al_2O_3/(Na_2O + K_2O)$ diagram (Shand, 1927). **(b, c)** Trace element discrimination diagrams (Nb–Y and Rb vs. Y+Nb) for syenodioritic pluton rocks (fields from Pearce et al., 1984; VAG = volcanic arc granites, WPG = within-plate granites, ORG = ocean ridge granites. SYN-COLG = syn-collisional granites. **(d)** Ti–Zr–Y diagram. **(e)** Ti–V diagram. **(f)** TiO_2 vs. Al_2O_3 diagram. **(g)** Y vs. Zr diagram. **(h)** Th/Yb vs. Nb/Yb diagram (fields after Pearce and Cann, 1973; Shervais, 1982; Muller et al., 1992; Pearce, 2008).

SED
5, 1941–2004, 2013

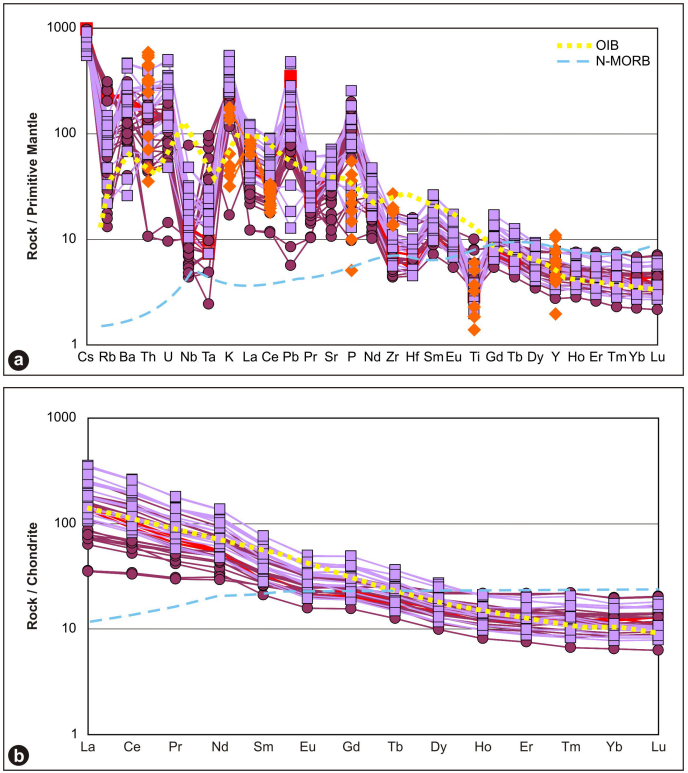

Fig. 17. (a) Primitive mantle-normalized multi-element diagrams for the high-K shoshonitic arc rocks (normalization values from Sun and McDonough, 1989). **(b)** Chondrite-normalized REE patterns of the same rocks (normalization values from Sun and McDonough, 1989).

SED
5, 1941–2004, 2013

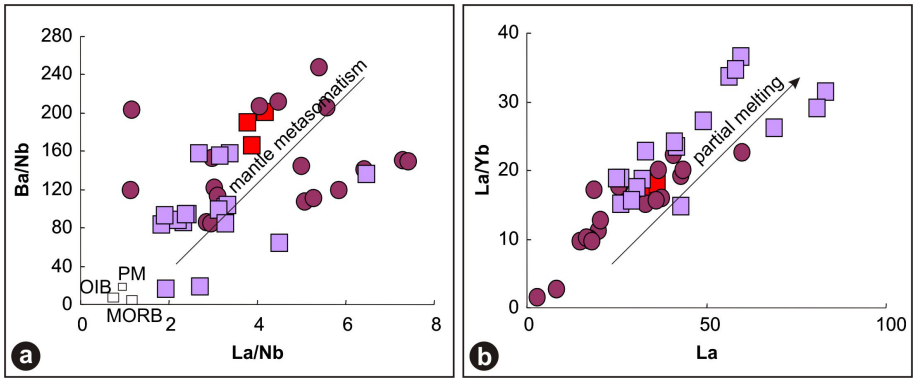

Fig. 18. (a) Ba/Nb vs. La/Nb diagram for the high-K island arc rocks. The data for N-MORB, OIB and PM are from Sun and McDonough (1989). **(b)** La/Yb vs. La diagram for the island-arc rock units, illustrating the effects of partial melting and fractionation in their melt evolution.

SED
5, 1941–2004, 2013

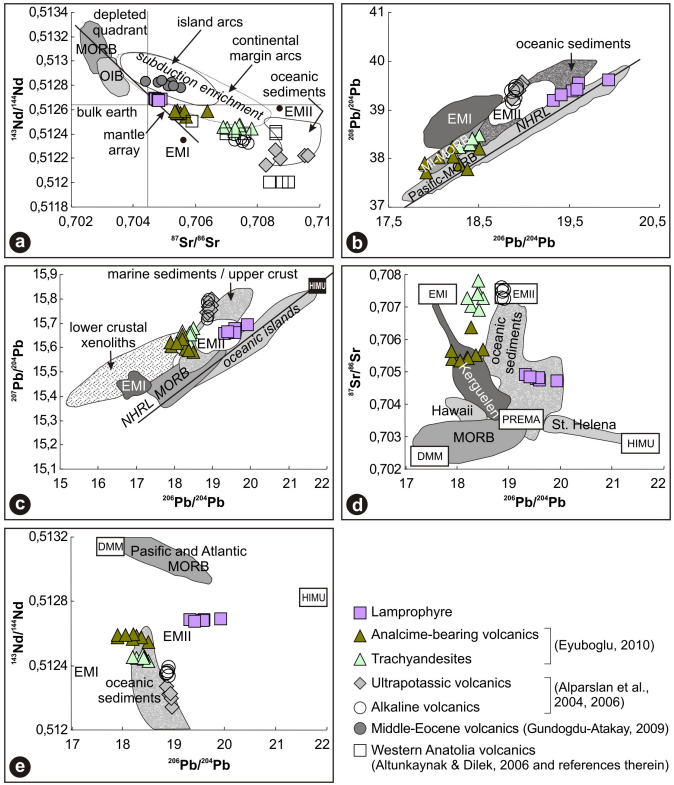

Fig. 19. Isotope variation diagrams for the Upper Cretaceous–Lower Paleocene high-K island-arc rocks. **(a)** $^{143}Nd/^{144}Nd$ vs. $^{87}Sr/^{86}Sr$ diagram. **(b)** $^{206}Pb/^{204}Pb$ vs. $^{208}Pb/^{204}Pb$ diagram. **(c)** $^{206}Pb/^{204}Pb$ vs. $^{207}Pb/^{204}Pb$ diagram. **(d)** $^{87}Sr/^{86}Sr$ vs. $^{206}Pb/^{204}Pb$ diagram. **(e)** $^{143}Nd/^{144}Nd$ vs. $^{206}Pb/^{204}Pb$ diagram. Compositional fields for the upper and lower crust, MORB (mid-ocean ridge basalt), HIMU (enriched mantle in U and Th relative to Pb), OIB (ocean island basalt), EMI (enriched mantle I) and EMII (enriched mantle II) are from Zindler and Hart (1986). The field for *Oceanic Islands* is from White (1985). NHRL = Northern Hemisphere Reference Line.

SED
5, 1941–2004, 2013

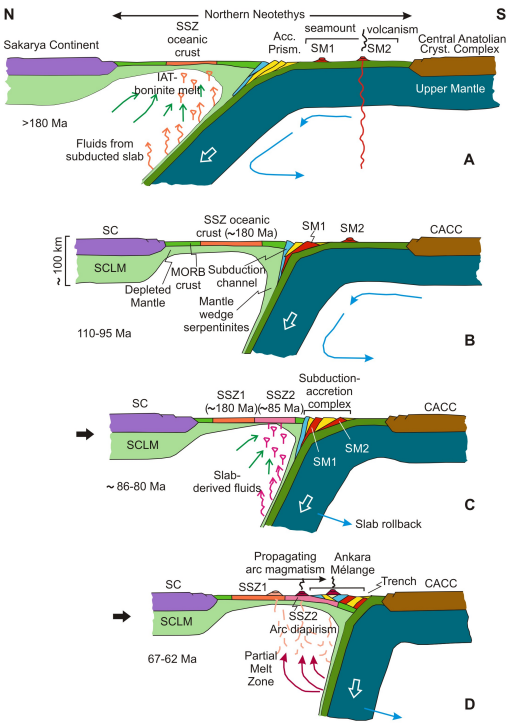

Fig. 20. Sequential tectonic diagrams depicting the intra-oceanic magmatic evolution of the Ankara Mélange in the Northern Neotethys during the Jurassic–Paleocene. **(A)** Suprasubduction zone generation of the oldest Neotethyan oceanic crust (~180 Ma) in the upper plate of a north-dipping intra-oceanic subduction zone, and seamount construction (SM1 and SM2) in the downgoing oceanic plate. High-grade metamorphic rock blocks and turbiditic sandstone-mudstone sequences in the Ankara Mélange formed in the subduction channel (blue in color) and the accretionary prism, respectively. **(B)** Accretion of Seamount-1 into the accretionary complex and related deformation in the subduction-accretion system. **(C)** Slab rollback and associated extension and SSZ oceanic crust formation (~85–80 Ma) in the upper plate. Accretion of Seamount-2 into the accretionary complex, and the lateral growth and deformation in the subduction-accretion system. **(D)** Island arc construction and magmatism on and across the pre-existing SSZ oceanic lithosphere and the subduction-accretion complex (i.e. Ankara Mélange units). With continued slab retreat, arc magmatism shifts southward following the migrating trench, and becomes more alkaline in time, producing lamprophyric and syeno-dioritic intrusions. See text for further explanation.

SED
5, 1941–2004, 2013